Stomatal Function across Temporal and Spatial Scales: Deep-Time Trends, Land-Atmosphere Coupling and Global Models[1][OPEN]

Peter J. Franks*, Joseph A. Berry, Danica L. Lombardozzi, and Gordon B. Bonan

Faculty of Agriculture and Environment, University of Sydney, Sydney, New South Wales 2006, Australia (P.J.F.); Department of Global Ecology, Carnegie Institution for Science, Stanford, California 94305 (J.A.B.); and National Center for Atmospheric Research, Boulder, Colorado 80307 (D.L.L., G.B.B.)

ORCID IDs: 0000-0002-4810-658X (P.J.F.); 0000-0002-5849-6438 (J.A.B.); 0000-0003-3557-7929 (D.L.L.).

The colonization of land by plants and their interaction with biogeochemical and atmospheric processes transformed continental climate and hydrology. Stomata, which evolved to optimize the biological economics of plant carbon uptake in exchange for water loss, play a crucial role in large-scale environmental processes by maintaining a connection between deep soil water reservoirs and the atmosphere, regulating terrestrial carbon sinks and altering surface energy balance as they respond to environmental changes. Stomatal feedback control of leaf gas exchange is observed at multiple temporal and spatial scales, but accurately simulating this dynamic behavior remains challenging, particularly for extreme environmental conditions, including drought. Integration of a more realistic representation of stomatal conductance and its regulation of leaf gas exchange in global models is improving global simulations of carbon, water, and energy fluxes, and these simulations in turn highlight some of the limitations with current leaf-scale models. Our analysis of current leaf-scale models of stomatal conductance representing empirical-based and optimization-based approaches reveals close structural similarities that result in virtually indistinguishable simulations of leaf, canopy, and global fluxes. While acknowledging these similarities, future efforts must focus on more accurate parameterization of stomatal conductance models, informed by studies at multiple temporal and spatial scales, including molecular, fossil, geological, leaf, canopy, and landscape.

Stomata first appeared more than 410 million years ago in rudimentary terrestrial plants (Edwards et al., 1998; Raven, 2002; Chater et al., 2016). From then on, they have significantly influenced the fluxes of carbon, water, and energy at the land surface (Berry et al., 2010). After gaining a foothold on land in the late Silurian (Edwards, 1998), the evolution and spread of vascular plants drove one of the most dramatic global climate change events in Earth's history.

The role of plants in changing Earth's climate was 2-fold: (1) the proliferation of deep-rooting systems and the uptake of nutrients throughout the Devonian enhanced the weathering of Ca-Mg silicate minerals, which facilitated the large-scale transfer of CO_2 from the atmosphere to marine carbonates; and (2) unprecedented production of lignin-rich, decay-resistant plant structural material, in conjunction with tectonic basins and wet tropical climates, sequestered massive amounts of carbon in vast coal deposits (Berner, 1997, 2005). The resulting massive drawdown in global atmospheric CO_2 concentration from many times that of today, via its reduction of the greenhouse effect, is likely to have contributed significantly to the Permo-Carboniferous glaciation (Royer et al., 2004; Lowry et al., 2014), the most extensive and longest lived glaciation since that time (Crowell, 1978; Scheffler et al., 2003; Montañez and Poulsen, 2013). Ultimately, strong negative feedbacks involving the limitation of terrestrial plant productivity and weathering by low CO_2 are likely to have stabilized minimum atmospheric CO_2 concentrations above the threshold for severe icehouse conditions (Pagani et al., 2009; Beerling et al., 2012). These megacycles in global vegetation productivity and atmospheric CO_2 concentration also are imprinted in the record of plant genome size evolution (Franks et al., 2012a).

The colonization of land by plants and extensive greening of the continents marked a dramatic shift in global water and carbon cycles that moderated continental climates and supported a diversity of terrestrial ecosystems (Kleidon et al., 2000; Beerling, 2007; Berry et al., 2010). Stomata played a crucial role in this by maintaining the flow of water from deep soil reservoirs back to the atmosphere, enhancing continental water cycling and cooling of the climate (Berry et al., 2010), a process that continues across terrestrial biomes today

[1] This work was supported by the Australian Research Council (to P.J.F., G.B.B., and J.A.B.), the National Center for Atmospheric Research (to P.J.F., D.L.L., and G.B.B.), and the National Institute of Food and Agriculture/U.S. Department of Agriculture (grant no. 2015-67003-23485 to G.B.B. and D.L.L.).

* Address correspondence to peter.franks@sydney.edu.au.

P.J.F., G.B.B., and J.A.B. conceived the research project; P.J.F., G.B.B., and D.L.L. conducted the analysis; P.J.F. and G.B.B. wrote the article with input from the other authors.

[OPEN] Articles can be viewed without a subscription.
www.plantphysiol.org/cgi/doi/10.1104/pp.17.00287

ADVANCES

- The colonization of land by plants established and maintained a connection between deep soil water reservoirs and the atmosphere that fundamentally altered global climate.
- Stomatal closure in response to increasing atmospheric CO_2 concentration is part of the negative feedback control of leaf gas exchange, but at the landscape scale the associated increase in canopy temperature constitutes a positive feedback or "physiological forcing" that amplifies the radiative forcing of CO_2 in the atmosphere.
- Extensive preservation of stomata in the fossil record allows reconstruction of atmospheric CO_2 concentration over the past 410 million years and reveals a coevolution of leaf gas exchange capacity with global climate.
- The universal negative relationship between stomatal size and density reflects a spatial optimization that minimizes allocation of epidermal area to stomata while maximizing diffusive conductance and underlies selection for higher stomatal conductance under declining atmospheric CO_2 concentration.
- Identification of key stomatal sensitivities and molecular signaling networks in all plant divisions points to a universal, ancient stomatal control mechanism.
- Models of stomatal conductance implemented at large scales are typically characterized by a single critical fitted parameter representing intrinsic water-use efficiency. Three common examples are the "Ball-Berry" model slope parameter (g_1 in Eq. 1; Ball et al., 1987), the "Medlyn" model slope parameter (g_{1M} in Eq. 3; Medlyn et al., 2011), and the water-use optimization gain ratio λ (as determined with *simplified* optimization models; e.g. Lloyd, 1991).
- Model simulations show that stomatal sensitivity to CO_2 over a defined range decreases with increasing ratio of maximum potential electron transport rate to maximum RuBP carboxylation rate, J_{max}/V_{cmax}.
- In addition to J_{max}/V_{cmax}, adaptation of stomata to changes in atmospheric CO_2 concentration may be reflected in changes in model parameters g_1, g_{1M}, and λ.
- Ball-Berry-type and simplified optimization-type dynamic stomatal conductance models are structurally similar and can produce similar outputs at leaf, canopy, and global scales if the input parameters are prescribed comparably. Differences in outputs between models emerge for extreme conditions (e.g. extremely moist or dry).
- Global models of water, carbon, and energy fluxes have been greatly improved by inclusion of dynamic models for stomatal conductance.

(Bonan et al., 1992; Snyder et al., 2004; Feddema et al., 2005; Bala et al., 2007; Arneth et al., 2010).

Under current increasing atmospheric CO_2 concentration, stomata continue to influence climate as a result of their primary role in optimizing plant water use. Stomatal closure in response to elevated CO_2 is a water-conserving mechanism that reduces transpiration but, as a consequence, increases canopy temperature. This physiological forcing adds to the radiative forcing effect of increasing atmospheric CO_2 concentration on climate (Sellers et al., 1996a; Betts et al., 1997; Cao et al., 2010). The potential magnitude of physiological climate forcing varies substantially from tropical to temperate to boreal landscapes (Bonan, 2008). However, its mechanism is not fully understood, particularly with regard to the role of vegetation in land-atmosphere coupling (Andrews et al., 2011; Berg et al., 2016; Byrne and O'Gorman, 2016).

Owing to the physical and chemical resilience of the guard cell wall and cuticle, stomata are well preserved in fossil plant remains through at least the last 410 million years of the geologic record (Beerling and Woodward, 1997). This resource has proven to be a valuable key to unlocking the history of vegetation-climate coevolution through the Phanerozoic because it has enabled reconstruction of the evolution of plant gas-exchange capacity and productivity (Beerling and Woodward, 1997; Franks and Beerling, 2009a) as well as global atmospheric CO_2 concentration (McElwain et al., 1999; Beerling and Royer, 2002; Grein et al., 2011; Franks et al., 2014; Montañez et al., 2016), the latter a critical boundary condition for simulating paleoclimates using global climate models (Kiehl and Shields, 2013; Meissner et al., 2014; Upchurch et al., 2015).

Despite these advances, the record of Earth's vegetation-climate coevolution is incomplete, with significant knowledge gaps remaining at some of the key periods of global transition (Montañez et al., 2016). Next-generation stomatal gas-exchange CO_2 proxy models are now helping to reduce uncertainty in reconstructed paleoatmospheric CO_2 concentration (Franks et al., 2014). Results from these studies are revising paleo-CO_2 estimates that were once widely disparate (e.g. 200–2,800 μmol mol^{-1} for the Paleocene-Eocene thermal maximum; McInerney and Wing, 2011) to well-constrained values that are more compatible with global paleoclimate simulations (Meissner et al., 2014; Upchurch et al., 2015). However, current paleo-CO_2 proxy methods and paleoclimate simulations require refinement and improvement to achieve better agreement across studies and to reduce uncertainty in model outputs.

The scales of stomatal influence are illustrated in Figure 1, with examples of some of the quantities involved and some of the tools applied to different spatial and temporal scales of study. Together with the diversity of technologies involved in data collection at multiple scales, robust, well-validated physiological models describing the complex behavior of stomata at the leaf level are essential for interpretation and simulation. Understanding and predicting larger scale carbon, water, and energy cycles requires accurate estimates of the leaf diffusive (stomatal) conductances to water vapor and CO_2 (g_w and g_c, respectively [definitions for these and other terms are given in Table I]) using stomatal conductance models. Despite considerable progress in the development and application of these models, theoretical questions remain about some of the most basic stomatal sensitivities to environmental variables, such as the response to CO_2 and water deficit (Brodribb and McAdam, 2011; Chater et al., 2011; Ruszala et al., 2011; Franks, 2013; Lind et al., 2015; Franks and Britton-Harper, 2016).

One universally recognized feature across all scales of stomatal functioning is their role as feedback regulators (Fig. 1; see discussion in Franks et al., 2013). Importantly, stomata behave as both negative and positive feedback elements, depending on the process. In their primary role of maintaining leaf hydration and optimizing the biological economics of photosynthesis, stomata are finely tuned negative feedback control systems. But, as noted above, the effects of this negative feedback control at the leaf level are manifested as a positive feedback or forcing of climate processes at the landscape scale. Accurately accounting for the effects of stomatal physiology at larger scales remains a challenge.

Here, we provide an update on stomatal function and patterns of change across temporal and spatial scales, with an emphasis on methods used to account for the role of stomata when simulating global carbon, water, and energy fluxes in global models. The temporal scale spans seasonal to evolutionary adaptation over millions of years, and the spatial scale spans leaf to globe.

STOMATAL SIZE, DENSITY, AND CONDUCTANCE THROUGH DEEP TIME

The fossil record reveals strong patterns of change in stomatal morphological features through major geological periods (Edwards et al., 1998; Franks and

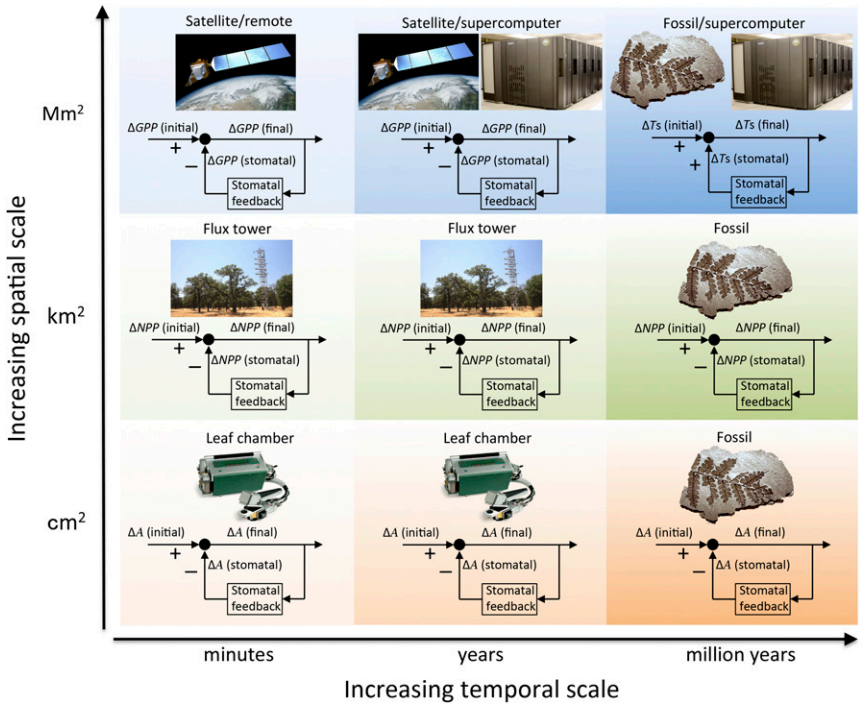

Figure 1. The scales of influence of stomata. Across temporal and spatial scales of study, there is a progression in the tools and technologies employed. Examples illustrated are leaf gas-exchange chamber, eddy flux tower, satellite, supercomputer, and fossils, the latter a form of deep-time climate data logger. Illustrated also are examples of the influence of stomatal feedback responses to perturbations at all scales. Quantities represented are change in net CO_2 assimilation rate (ΔA), change in net primary productivity (ΔNPP), change in global gross primary productivity (ΔGPP), and change in global surface temperature (ΔTs). The typical relative direction of change is illustrated with plus and minus symbols. Note the positive (amplifying) feedback effect of stomata on ΔTs (top right).

Table I. *List of symbols with description and units*

Symbol	Description	Units
A	Net CO_2 assimilation rate	μmol m^{-2} s^{-1}
A_c	RuBP carboxylation-limited CO_2 assimilation rate	μmol m^{-2} s^{-1}
A_j	RuBP regeneration-limited CO_2 assimilation rate	μmol m^{-2} s^{-1}
A/E	Water-use efficiency	mmol CO_2 mol^{-1} water
c_a	CO_2 concentration of the atmosphere	μmol mol^{-1}
c_i/c_a	Ratio of intercellular to atmospheric CO_2 concentration	Dimensionless
c_i	Leaf intercellular CO_2 concentration	μmol mol^{-1}
c_s	CO_2 concentration at the leaf surface	μmol mol^{-1}
D	Stomatal density	mm^{-2}
D_s	Leaf-to-air vapor pressure difference at the leaf surface	kPa
D_0	Fitted parameter in Equation 2	kPa
E	Transpiration rate	mol m^{-2} s^{-1}
g_{bc}	Leaf boundary layer conductance to CO_2	mol m^{-2} s^{-1}
g_c	Stomatal conductance to CO_2	mol m^{-2} s^{-1}
$g_{c(max)}$	Maximum stomatal conductance to CO_2	mol m^{-2} s^{-1}
g_w	Stomatal conductance to water vapor	mol m^{-2} s^{-1}
$g_{w(max)}$	Maximum stomatal conductance to water vapor	mol m^{-2} s^{-1}
g_0	Intercept in Equations 1, 2, and 3, representing minimum g_w	mol m^{-2} s^{-1}
g_1	Slope in Equation 1 (a fitted parameter)	Dimensionless
g_{1M}	Fitted parameter in Equation 3	$(kPa)^{0.5}$
H	Relative humidity at the leaf surface (as a fraction)	Dimensionless
J_{max}	Maximum potential electron transport rate	μmol m^{-2} s^{-1}
R_d	Leaf respiration rate	μmol m^{-2} s^{-1}
S	Stomatal size	μm^2
V_{cmax}	Maximum RuBP carboxylation rate	μmol m^{-2} s^{-1}
$\partial A/\partial g_w$	Sensitivity of A to g_w	mmol mol^{-1}
$\partial E/\partial g_w$	Sensitivity of E to g_w	mmol mol^{-1}
$\partial E/\partial A$	Sensitivity of E to A, or gain ratio	mmol water μmol^{-1} CO_2
Γ	CO_2 compensation point including respiration	μmol mol^{-1}
Γ^*	CO_2 compensation point without dark respiration	μmol mol^{-1}
λ	Marginal water cost of leaf carbon	mmol water μmol^{-1} CO_2

Beerling, 2009b). The implications from this, based on the well-established coupling between vegetation and climate (Bonan, 2016) and the influence of stomatal morphology on leaf gas exchange (Franks and Farquhar, 2007), are that these patterns reflect coordinated shifts in global vegetation and climate. One challenge, therefore, has been to understand the driving forces and mechanisms behind these patterns, particularly in the context of what they can reveal about the current phase of Earth's environmental transition.

Some of the earliest insights came from the observation that stomatal density (D; number per unit of area) in leaf material preserved over the last two centuries is negatively correlated with the increase in atmospheric CO_2 concentration (c_a) over that time (Woodward, 1987). It is now well established from controlled-environment studies at elevated and subambient c_a that, over time frames as short as the development and expansion of a leaf, plants can adjust D in response to a sustained change in c_a. This adaptation is usually in the direction that would tend to counteract the physiological effects of the change in c_a (e.g. higher D with lower c_a increases stomatal conductance to counteract the initial drop in CO_2 assimilation rate; Franks et al., 2012b, 2013). What remains unclear about this simple principle is how to characterize this sensitivity quantitatively for the purpose of simulation or prediction.

Modeling the response of D to change in c_a has proven difficult. At developmental time scales, there are strong species-specific differences in sensitivity, including cases of apparent insensitivity (Reid et al., 2003; Tricker et al., 2005; Haworth et al., 2015), as well as nonlinearities in the response over both developmental and evolutionary time scales (Franks et al., 2013). This has been especially problematic in attempts to use the change in D in leaf fossils, alone, as a proxy for change in global mean c_a (Royer, 2014). A detailed theoretical framework for modeling the response of D to c_a has been proposed that uses principles of leaf gas-exchange optimization (Konrad et al., 2008), but this awaits broader implementation and validation.

Early studies suggested that the sensitivity of D to c_a was substantial. For example, Woodward (1987) found that D decreased by 40% to 67% for both historic and growth chamber-simulated change in c_a from 280 to 340 μL L^{-1}, a rate of 66% to 112% per 100 μL L^{-1}, assuming an approximately linear response in this relatively narrow range of c_a. From the many hundreds of studies that have followed, it appears that the sensitivity is usually much less than this, perhaps as little as 2% to 4% per 100 μL L^{-1} increase in c_a on average (Franks et al., 2012b). This relatively moderate mean sensitivity of D to c_a should be considered in the

interpretation of studies involving the manipulation of c_a, particularly where c_a is changed by only a couple of hundred microliters per liter, as in many free-air CO_2 enrichment (FACE) studies.

A key insight to emerge in studying the effects of changing c_a on stomatal density is its coordination with stomatal size (S) and, ultimately, the anatomical maximum diffusive conductance to CO_2 and water vapor [$g_{c(max)}$ and $g_{w(max)}$, respectively]. Changes in D appear to be inextricably linked to changes in S, and it is the combination of S and D that determines $g_{c(max)}$ and $g_{w(max)}$. There is a consistent negative relationship between S and D at all scales, including leaves within a single species (Franks et al., 2009), across species in a population (Hetherington and Woodward, 2003; Russo et al., 2010), through the fossil record (Franks and Beerling, 2009b), and across mutants of a single species where D is induced to vary by genetic manipulation (Doheny-Adams et al., 2012; Dow et al., 2014; Franks et al., 2015). This negative logarithmic relationship (often represented as a negative linear log-log plot) fundamentally constrains the adaptation and evolution of stomata under forcing by any environmental variable affecting leaf gas exchange. To achieve a new $g_{c(max)}$ and $g_{w(max)}$, plants alter S and D within the confines of a general negative logarithmic relationship that optimizes the allocation of leaf epidermal area to gas exchange (de Boer et al., 2016). Fundamentally, selection for higher stomatal conductance is linked to lower S and higher D (Franks and Beerling, 2009b)

The optimization strategy identified by de Boer et al. (2016) has its own set of physical constraints, imposed by the biochemical and mechanical requirements of stomata and the size of the genome that is packed into the nucleus of each guard cell. To be fully functional, stomata need to be separated by at least one epidermal cell, the so-called one-cell-spacing rule (Geisler et al., 2000; Dow et al., 2014), and stomatal guard cells cannot be any smaller than their nucleus. Across vascular plants, much of the greater than 40-fold range in stomatal size (length × width) and, hence, maximum stomatal conductance (Franks and Beerling, 2009b) is linked to the evolution of plant genome size (Beaulieu et al., 2008; Knight and Beaulieu, 2008; Franks et al., 2012a), and angiosperms span the broadest range. This widely observed correlation between stomatal size, guard cell nucleus size, and plant genome size has prompted the hypothesis (yet to be tested comprehensively) that selection for higher or lower stomatal conductance involves coselection for correlated changes in S, D, and genome size (Franks et al., 2012a, 2012b). The role of factors that determine nucleus size and architecture also must be considered, including coiled-coil proteins in the Nuclear Matrix Constituent Protein family (Wang et al., 2013). If genome size does impose a constraint on stomatal size and gas-exchange capacity, then the wide range of angiosperm genome size could be a significant contributing factor in the current dominance of angiosperms across diverse landscapes and climates.

STOMATA EVOLVED AS LAND PLANTS DIVERSIFIED, BUT ALL PLANT DIVISIONS MAY EXHIBIT COMMON STOMATAL CONTROL ATTRIBUTES

One of the most important areas of recent research focus has been the evolution of the stomatal control system, in particular the timing of emergence of active stomatal responses to CO_2 and water deficit as well as mediation by the stress hormone abscisic acid (ABA). This is important because biophysical and molecular models of stomatal control rely upon assumptions about the presence and characteristics of core sensitivities and signaling pathways.

A series of studies have proposed that stomatal sensitivity to CO_2 and ABA evolved first in seed plants (angiosperms and gymnosperms) and are absent in lower vascular plants of more ancient origin, such as ferns and lycophytes (Brodribb et al., 2009; Brodribb and McAdam, 2011, 2013; McAdam and Brodribb, 2012, 2015). These studies hypothesize that, before the evolution of seed plants, stomatal control, particularly in response to water deficit, was largely hydropassive (referred to here as the passive origin model, after Brodribb and McAdam, 2011; also described as the gradualistic model in McAdam and Brodribb, 2012). This hypothesis has been rejected in a number of studies utilizing a variety of methods, including cross-species genetic complementation, bioinformatics, and leaf gas-exchange measurements, which together suggest that active stomatal sensitivity to ABA and CO_2 are traits common to all major land plant divisions (Chater et al., 2011; Ruszala et al., 2011; Lind et al., 2015; Franks and Britton-Harper, 2016; Cai et al., 2017; Chen et al., 2017).

If similar active and passive control elements are identified in all major land plant divisions, this would suggest that they share essentially one stomatal control mechanism (Franks and Britton-Harper, 2016). This universal or general model for stomatal control is illustrated conceptually in Figure 2. In comparison, the passive origin or gradualistic model can be viewed as a variant of the general model in which all of the gene regulatory networks and behaviors associated with the active stomatal response to elevated CO_2 and water deficit are absent from seedless plants (but now updated to include CO_2 sensitivity in ferns and gymnosperms, after Franks and Britton-Harper, 2016; see red colors in Fig. 2). However, some disagreement remains on whether stomatal ABA sensitivity is universal (McAdam et al., 2016).

A general model incorporating active and passive control in all land plants does not imply or predict identical or uniform stomatal behavior. It does, however, incorporate the operation of similar genetic systems, molecular signaling pathways, and feedback control loops in stomata of nonangiosperms as well as angiosperms. All of these elements will have been subjected to natural selection as land plants diversified, and, as a result, many will exhibit altered characteristics among plant clades. However, like the shared basic

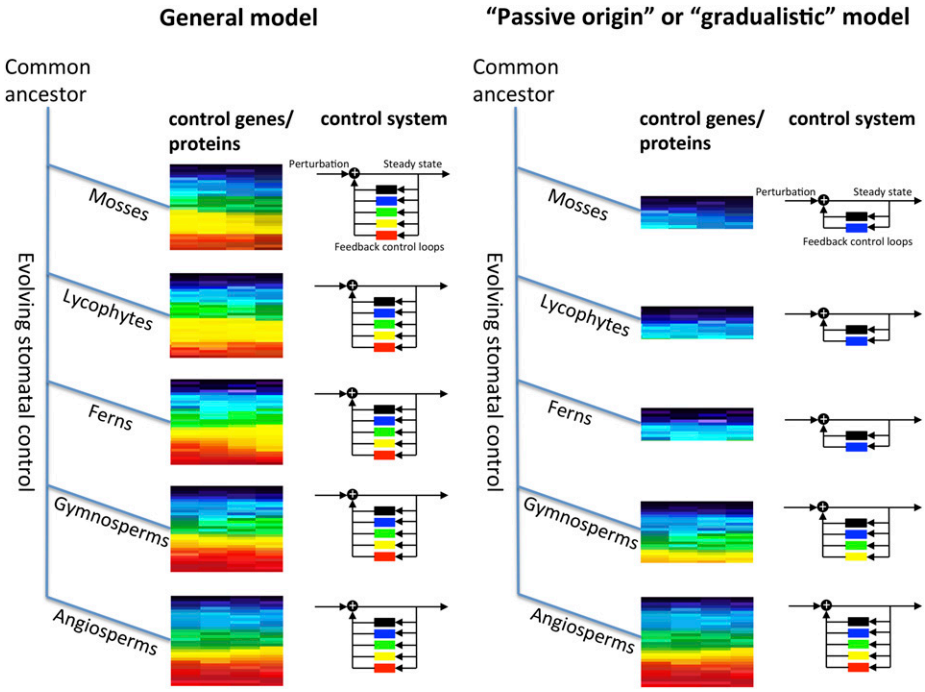

Figure 2. Illustrating two current models for the evolution of stomatal control: the general and passive origin (or gradualistic) models. Both models describe the key elements of the stomatal control system and the evolution of these elements as new plant lineages emerged. The major plant divisions, all with stomata, are arranged phylogenetically with respect to their common ancestor (distances not to scale). The main difference between the two models is that the general model incorporates, in some form, all of the core elements of passive and active stomatal control in each plant division, whereas the passive origin (or gradualistic) model assumes that certain active stomatal control elements, including sensitivity to elevated CO_2 and ABA, evolved first in angiosperms (possibly gymnosperms in the case of ABA sensitivity) and are absent in all other divisions. Colors represent genes, gene families, or gene regulatory networks involved in discrete elements of the stomatal control system and their respective feedback control loops in the regulation of stomatal conductance; different color hues represent homologs or other variants resulting from evolutionary processes: black = active response to light; blue = passive response to water potential; green = active response to water potential (including changes imposed by vapor pressure difference); yellow = active ABA response; and red = active response to elevated CO_2.

form and mechanical function of stomata in all land plant divisions (two guard cells that bend apart with increased turgor to create an aperture for gas exchange), a general stomatal control model applies a basic mechanistic framework to the subcellular and extracellular processes that govern stomatal aperture. Further definitive genic and physiological information is needed to fully characterize the origins and nature of passive and active stomatal control across the diversity of vascular plants.

MODELING STOMATAL CONDUCTANCE AT ALL SCALES IS UNDERPINNED BY AN ACCURATE MECHANISTIC UNDERSTANDING

Predicting and manipulating plant gas exchange requires a mechanistic understanding of the process. Goal-driven manipulation (genetic, biochemical, or otherwise) of the behavior of stomata for the purpose of modifying plant gas exchange requires some understanding of the stomatal control mechanism and its elements (genes, signaling networks, internal conductances, etc.). In turn, accurate mechanistic models of stomatal function built from observations of cellular processes can inform the behavior of higher order leaf gas-exchange processes. An example is the OnGuard computational platform for kinetic modeling of guard cell physiology (Hills et al., 2012). Built from detailed observations of guard cell biophysical and kinetic processes, OnGuard has been shown not only to simulate the behavior of stomata but to predict previously unrealized biophysical processes within the guard cell that were subsequently verified experimentally, thus improving the understanding of higher order stomatal function (Chen et al., 2012; Wang et al., 2014). Application of this approach more generally across plant divisions depends on accurate characterization of the subcellular processes governing stomatal behavior in all plant divisions. If some of these processes are found to be lacking in certain plants, then the configuration and broader application of models like OnGuard will have to be revised.

Stomatal conductance models applied to larger spatial scales fall into three broad categories: semiempirical (Jarvis, 1976; Ball et al., 1987), semimechanistic (Buckley et al., 2003), and semioptimization (Lloyd, 1991; Katul

et al., 2009; Medlyn et al., 2011). The prefix semi applies because empirical stomatal conductance models are actually founded on solid physiological theory, and all practical applications of mechanistic and optimization models require empirical or other mathematical simplifications, so, in practice, none of the models fits purely into one category. Regardless of classification, each approach has delivered considerable success, but there is now a growing interest in reexamining the merits of these approaches and exploring possible improvements, with particular emphasis on optimization.

Although several innovative studies have applied optimization theory to model plant gas exchange (Lloyd and Farquhar, 1994; Buckley, 2008; Katul et al., 2010; Medlyn et al., 2011; Bonan et al., 2014), it has not been as widely adopted as might have been expected from such an elegant theory. Stomatal control of leaf gas exchange was formulated in terms of optimization theory almost four decades ago (Cowan and Farquhar, 1977), but stomatal control has been modeled predominantly using semiempirical or hybrid mechanistic-empirical approaches (Damour et al., 2010). One difficulty with the practical application of optimization theory is quantifying the ratio of sensitivities of the rates of transpiration (E) and CO_2 assimilation (A) to changes in stomatal conductance to water vapor (g_w), defined as the gain ratio $(\partial E/\partial g_w)/(\partial A/\partial g_w)$, or simply $\partial E/\partial A$ (Farquhar et al., 1980a). Stomatal conductance behaves optimally when $\partial E/\partial A$ is maintained at some constant value, λ. But what determines λ, or what should it be? Stomatal optimization theory cannot provide these answers, it only allows us to determine whether the plant has achieved a given requirement of photosynthetic assimilate with the least possible transpirational loss of water in an environment with certain statistical properties (Cowan and Farquhar, 1977). Cowan (2002) remarked on the potentially indefinable nature of this problem, which takes the form of a fruitless search for optimal λ, appealing to ever-higher levels of plant organization and requiring increasingly dubious simplifications to make the problem tractable.

As a way forward, methods have been devised for prescribing or estimating λ for use in gas-exchange models employing stomatal optimization, but this requires some empirical or mechanistic insight into the nature of E, A, and g_w in the plant or vegetation of interest as well as a number of simplifications that may be unrealistic and/or inconsistent with the original Cowan-Farquhar optimization theory (Buckley et al., 2017). This is somewhat analogous to prescribing c_i/c_a (the ratio of intercellular to atmospheric CO_2 concentration) for a mechanistic model or the slope parameter g_1 in the empirically based Ball-Berry (BB) model (Ball et al., 1987; see Eq. 1 below). The widely observed relative constancy of c_i/c_a for a leaf under typical daily conditions, a feature predicted by the optimal control of stomatal conductance for some conditions, has been usefully applied in the modeling of plant gas exchange, including over geological time (Franks et al., 2014). Note that c_i/c_a does exhibit some systematic variation: it declines with water deficit (Farquhar et al., 1989), and across species, it tends to be higher in plants with greater photosynthetic capacity (Franks and Farquhar, 1999). Although c_i/c_a is mechanistically defined and readily measured, as with λ it is not clear what ultimately determines c_i/c_a. Furthermore, for any value of λ, the trajectories of E, A, and g_w depend on plant metabolic and biophysical attributes that, for the purpose of simulation or prediction, must be defined mechanistically or empirically and calibrated for the plant or vegetation of interest. Errors in the characterization of these traits in different plant functional types will limit the capacity of optimization-type stomatal models to simulate or predict plant gas exchange. Therefore, caution must be used when assessing the benefits of optimization approaches compared with other methods.

STOMATA IN GLOBAL MODELS: EMPIRICAL AND OPTIMIZATION APPROACHES ARE STRUCTURALLY SIMILAR AND CAN PROVIDE IDENTICAL OUTPUTS

Land surface models simulate the fluxes of momentum, energy, moisture, and CO_2 between the land and atmosphere. These models, when coupled with models of atmospheric general circulation, ocean general circulation, and sea ice, form the terrestrial component of Earth system models. Central to Earth system models is the regulation of transpiration and photosynthesis by stomata.

Early versions of land surface models (Dickinson et al., 1986; Sellers et al., 1986) used a maximum stomatal conductance that was multiplicatively scaled for photosynthetically active radiation, temperature, vapor pressure deficit, soil water, and atmospheric CO_2 concentration using the framework of Jarvis (1976; see the commentary on early work by Jarvis in Beerling, 2015). Subsequent land surface models utilize empirical relationships between A and g_w to model stomatal conductance. In the BB model (Ball et al., 1987), for example,

$$g_w = g_0 + g_1 \frac{A}{c_s} H, \quad (1)$$

where A is net CO_2 assimilation rate (μmol CO_2 m^{-2} s^{-1}), c_s is the atmospheric CO_2 concentration at the leaf surface (μmol mol^{-1}), H is the relative humidity (expressed as a fraction) at the leaf surface, and stomatal conductance g_w has units (mol water m^{-2} s^{-1}). The slope parameter g_1 (dimensionless) relating g_w to AH/c_s is obtained by fitting the equation to leaf gas-exchange data, and the intercept of this regression, g_0, which is usually close to the origin, represents a minimum conductance (mol water m^{-2} s^{-1}).

The significance of g_1 is sometimes lost in referring to the BB model as an empirical model. However, it is readily apparent from Equation 1 that g_1 is largely

representative of the ratio g_w/A, the reciprocal of intrinsic water-use efficiency, A/g_w (Farquhar et al., 1989; Feng, 1999), and, therefore, also is related to actual water-use efficiency, A/E. Therefore, it might be expected that plants with characteristically higher A/E will exhibit lower g_1, and this has been observed (Kaminski et al., 2015). The quantity g_1, therefore, embodies the physiological traits that determine plant water-use efficiency.

The BB stomatal model was introduced into land surface models in the mid-1990s (Bonan, 1995; Sellers et al., 1996b; Cox et al., 1998) and is now commonly used to simulate stomatal conductance. To more accurately account for A as c_s approaches zero, Leuning (1990) modified the BB equation by replacing c_s with $c_s - \Gamma$, where Γ is the CO_2 compensation point for photosynthesis (including respiration in the light). Also, Equation 1 simulates a linear variation in g_w with change in humidity, so to simulate the often observed nonlinear variation in g_w with change in humidity, Leuning (1995) replaced H in Equation 1 with $(1 + D_s/D_0)^{-1}$,

$$g_w = g_0 + g_{1L}\frac{A}{(c_s - \Gamma)(1 + D_s/D_0)}, \quad (2)$$

where D_s is the vapor pressure deficit at the leaf surface, D_0 is an empirical parameter, and g_{1L} (dimensionless) is the equivalent of g_1 in Equation 1, although of different magnitude for the same conditions. Some models use this form of the BB equation (e.g. the Australian CABLE model; Wang et al., 2011).

Medlyn et al. (2011) introduced a third variant of Equation 1, hereafter abbreviated as the MED model,

$$g_w = g_0 + 1.6\left(1 + \frac{g_{1M}}{\sqrt{D_s}}\right)\frac{A}{c_s}, \quad (3)$$

where g_{1M} is a fitted parameter similar to g_1 in Equation 1, although of different magnitude for the same conditions, and with units that depend on those used for D_s: if D_s has partial pressure units (kPa), then g_{1M} has units $(\text{kPa})^{0.5}$; if D_s has mole fraction units (mmol mol^{-1}), then g_{1M} has units $(\text{mmol mol}^{-1})^{0.5}$. It should be noted that, unlike the straightforward determination of g_1 by linear regression, determining g_{1M} by fitting Equation 3 to data is a more complex procedure on account of nonlinearity. In Equation 3, g_w varies with humidity in a similar fashion to Equation 2, but as the inverse of the square root of D_s, as predicted by optimal stomatal behavior in response to D_s (see Appendix in Lloyd, 1991). Medlyn et al. (2011) define g_{1M} as,

$$g_{1M} = \sqrt{\frac{3\Gamma^*\lambda}{1.6}}, \quad (4)$$

where Γ^* is the CO_2 compensation point for photosynthesis without dark respiration, with units (μmol mol^{-1}), and λ is as defined earlier, with units (mmol water μmol^{-1} CO_2), following the original definition in terms of $\partial E/\partial A$ by Cowan and Farquhar (1977), which was also adopted by Medlyn et al. (2011). Note that, in the format of Equation 4, g_{1M} has units $(\text{mmol mol}^{-1})^{0.5}$, but this can be converted to $(\text{kPa})^{0.5}$ by dividing by $\sqrt{10}$, assuming atmospheric pressure of ~100 kPa. It is useful to note also that, for similar conditions of temperature and over a moderate range of relative humidity (~40%–80%), g_1 and g_{1M} are approximately related by

$$g_1 \approx \frac{1.6}{H}\left(1 + \frac{g_{1M}}{\sqrt{D_s}}\right). \quad (5)$$

The MED model relies upon several simplifications; most crucial is that it represents only the condition of ribulose 1,5-bisphosphate (RuBP) regeneration-limited photosynthesis. Medlyn et al. (2011) justify this by arguing, on the basis of observations, that stomata appear to behave as if to optimize RuBP regeneration-limited photosynthesis. Cowan and Farquhar (1977) also remarked on this puzzling behavior and noted that, whatever the physiological mechanism is for maintaining λ constant, the apparent tendency of stomata to optimize only RuBP regeneration-limited photosynthesis suggests that plants do not sense and respond to $\partial E/\partial A$ itself. This is a crucial insight that highlights the difficulty in describing λ in terms of the molecular signaling processes and actuating mechanisms driving stomatal control. The specificity of the MED model to the optimization of RuBP regeneration-limited photosynthesis is an important characteristic to consider when comparing the output of the MED model with a full water-use efficiency optimization model, as discussed below.

The significance of the MED model is that it is derived by combining the standard leaf diffusion equations with an equation for optimum leaf internal CO_2 concentration, c_i, in terms of the optimization criterion λ (Arneth et al., 2002), thereby linking g_1 to λ (as well as Γ^*, which is temperature dependent). This connection is intuitive because g_1, λ, and, therefore, g_{1M} are all indexes of plant water-use efficiency (or more precisely its reciprocal, E/A, as traditionally defined). However, compared with the BB model, the MED model offers a broader theoretical framework for developing predictive tools and testable hypotheses around plant water-use efficiency and its optimization. Fundamentally, though, the BB and MED models share the same physiological foundations.

Although the BB equation, and its variants (Eqs. 1–3), are based on a simple linear approximation of the relationship between g_w and A, its implementation in land surface models is complex. This first requires an estimate of A, which for C_3 plants is commonly represented using the Farquhar et al. (1980b) photosynthesis model. In that model

$$A = \min(A_C, A_j) - R_d, \quad (6)$$

where A_c is the Rubisco-limited CO_2 assimilation rate, A_j is the RuBP regeneration-limited CO_2 assimilation

rate, and R_d is the leaf respiration rate. The rates A_c and A_j depend on c_i, which itself depends on A and g_w through the leaf CO_2 diffusion equation

$$A = \frac{c_a - c_i}{g_c^{-1} + g_{bc}^{-1}}, \quad (7)$$

where g_{bc} is the leaf boundary layer conductance to CO_2 and g_c is the stomatal conductance to CO_2, equivalent to $g_w/1.6$ (Farquhar and Sharkey, 1982). This results in a system of three equations with three unknowns (A, g_w, and c_i). A further complication is that D_s and c_s, which are specific to the leaf surface, differ slightly from their values in the ambient air at some distance away from the leaf surface. This difference is determined by the boundary layer conductances to water and CO_2, respectively. Some models simplify the calculations by assuming an infinite boundary layer conductance, which effectively makes the values for humidity and CO_2 concentration at the leaf surface the same as those of ambient air. In this case, an analytical solution for g_w can be obtained for C_3 photosynthesis (Leuning, 1990). The solution finds the c_i that satisfies the equation set, which is then used to calculate A and g_w. The equation set must be solved twice, once to obtain c_i for the Rubisco-limited photosynthetic rate and again for the RuBP regeneration-limited rate. However, yet another complication is that the solution depends on leaf temperature (through D_s and also through metabolic parameters in the photosynthesis model) but leaf temperature depends on g_w. Iterative numerical solutions are needed to account for these dependences (Collatz et al., 1991).

An ongoing research topic is the extent to which the empirical-based BB-style equations represent more fundamental principles of water-use efficiency optimization. This theory, as postulated by Cowan and Farquhar (1977), states that optimization is achieved if

$$\frac{\partial A}{\partial g_w} = \frac{1}{\lambda}\frac{\partial E}{\partial g_w}, \quad (8)$$

where λ remains constant. An equation for g_w can be obtained from this relationship with A expressed in terms of the Farquhar et al. (1980b) photosynthesis model, but the form of the equation varies with the Rubisco and RuBP regeneration-limited rates of A (Arneth et al., 2002; Buckley et al., 2002; Katul et al., 2010; Medlyn et al., 2011; Vico et al., 2013; Buckley and Schymanski, 2014; Buckley et al., 2017). Although the utility of water-use efficiency optimization has been demonstrated in leaf gas-exchange studies, it has not been implemented directly in land surface models. One exception is the community land model (CLM), in which Bonan et al. (2014) evaluated a water-use efficiency optimization stomatal model at several forest sites. That study found that, without soil moisture stress, CLM simulations using the optimization-type stomatal conductance model performed similarly to those using the traditional BB stomatal conductance model, but the optimization approach improved the quality of CLM simulations under soil moisture stress.

Another important question is the relative significance of g_1, g_{1M}, and λ as diagnostic or physiologically descriptive traits. The ratio c_i/c_a, measured under normal (light-saturated) conditions of leaf gas exchange or as a time-integrated value from carbon isotope discrimination ($\Delta^{13}C$) in plant material, has long been recognized as an index of plant water-use efficiency. A decline in c_i/c_a [and $\Delta^{13}C$; i.e. an increase in $(1-c_i/c_a)$] is equivalent to an increase in A/E if c_s and D_s are constant (Farquhar et al., 1989). Assuming that $g_0 \approx 0$, the approximate relationship of mean c_i/c_a to g_1 in terms of H is

$$c_i/c_a \approx 1 - \frac{1.6}{g_1 H} \quad (9)$$

and to g_{1M} in terms of D_s is

$$c_i/c_a \approx 1 - \frac{\sqrt{D_s}}{\sqrt{D_s} + g_{1M}}. \quad (10)$$

The values for g_1, g_{1M}, and λ have been shown to vary severalfold across plant species, communities, and biomes (Lloyd and Farquhar, 1994; Baldocchi and Xu, 2005; Lin et al., 2015). The range of c_i/c_a is more conservative (Franks et al., 2013), but within these narrow limits, there is a systematic global trend toward lower c_i/c_a (increased water-use efficiency) with lower mean annual precipitation, as indicated by lower $\Delta^{13}C$ (Diefendorf et al., 2010). These ranges of variability are consistent with long-established differences in gas-exchange capacity and water-use efficiency across species (Schulze et al., 1994).

The primary explanation for this variability is illustrated in Figure 3A, which shows the global relationship between A and g_w for C_3 plants at current day (or near current day) atmospheric CO_2 concentration. A globally constant g_1, g_{1M}, λ, or c_i/c_a would require a constant ratio of A/g_w, but for C_3 plants globally, the mean ratio A/g_w decreases with increasing mean g_w (Fig. 3A). The pattern is not as pronounced for C_4 species, which, because of their internal CO_2-concentrating mechanism, typically maintain higher A than C_3 species for the same g_w. Therefore, C_3 plants with higher capacity for photosynthesis tend to exhibit lower A/g_w and higher g_1, g_{1M}, λ, and c_i/c_a. An example is shown in Figure 3B, where mean $(1 - c_i/c_a)$, an indicator of water-use efficiency, decreases with mean g_w globally across C_3 plants.

Remarkably, when the BB model (Eq. 1) is applied to the pooled data for C3 plants from all major biomes, represented by 276 species of trees, shrubs, grasses, and crops, a single g_1 value of 12.7 captures the gas-exchange behavior of global vegetation exceptionally well (Fig. 3C). It is for this reason that recent versions of CLM have, for convenience, applied a single value for

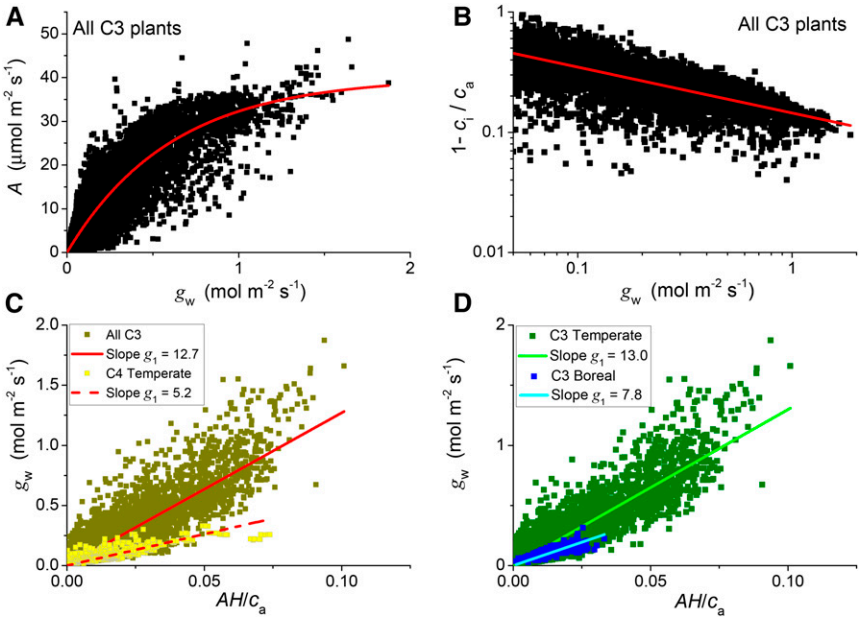

Figure 3. Global trends in leaf gas-exchange capacity and water-use efficiency. Each data point is an individual leaf-level measurement from raw data compiled by Lin et al. (2015). A, Global nonlinear relationship between CO_2 assimilation rate (A) and stomatal conductance to water vapor (g_w) for 276 species with C3 photosynthesis from all major biomes. Note that measurements are for ambient atmospheric CO_2 concentration (±60 μL L^{-1}) and cover a broad range of leaf temperature (5°C–45°C). The fitted line is $y = a - bc^x$, where $a = 40$, $b = 40$, $c = 0.19$, $n = 14{,}001$, $r^2 = 0.77$, $P = 0$. B, Global decline in mean $1 - c_i/c_a$, representing water-use efficiency, with increasing mean g_w, for species in A, using measurements above photosynthesis-saturating light (greater than 800 μmol m^{-2} s^{-1} photosynthetically active radiation). The fitted line is $y = 0.144x^{-0.38}$, $n = 6{,}784$, $r^2 = 0.5$, $P = 0$. C, Mean g_1 values obtained by fitting the BB model (Eq. 1, assuming $g_0 = 0$ and $c_s \approx c_a$, as in Lin et al., 2015) to subsets of the data from Lin et al. (2015), representing C3 plants (as in A) and C4 plants from a temperate semiarid biome. Data sampled are for the relative humidity (H) range 0.1 to 0.9. Fitted lines are as follows: C3 plants, $y = 12.7x$, $n = 12{,}521$, $r^2 = 0.87$, $P = 0$, solid red line; C4 plants, $y = 5.23x$, $n = 599$, 27 species, $r^2 = 0.86$, $P = 0$, dashed red line. D, Mean g_1 values obtained as in C for subsets of the C3 plants, showing different biome-specific g_1 values. Fitted lines are as follows: C3 temperate biome, $y = 13x$, $n = 11{,}010$, 74 species, $r^2 = 0.89$, $P = 0$, green line; boreal biome, $y = 7.8$, $n = 492$, five species, $r^2 = 0.95$, $P = 0$, blue line.

g_1 in global simulations. In CLM4.5, $g_1 = 9$ for C3 plants and $g_1 = 4$ for C4 plants (Bonan et al., 2011; Oleson et al., 2013), following Sellers et al. (1996b). A similar approach has been taken with CABLE, in which a single value of g_{1L} is applied (De Kauwe et al., 2015; Kala et al., 2015). CABLE also has been implemented with Equation 3 for g_w and assigning g_{1M} values according to the plant functional types in Lin et al. (2015). It is relatively straightforward to apply this approach also to CLM. Some potential values of g_1 specific to global biomes are illustrated in Figure 3D, comparing C3 temperate and boreal biomes. Using Equations 4, 5, and 9, it is possible to determine approximate equivalent values of λ, g_1, and mean c_i/c_a for corresponding values of g_{1M}, as shown in Table II. These four different indicators of water-use efficiency, therefore, share similar potential for use as calibrating elements in global models.

Leaf-Scale Simulations

Leaf-scale simulations illustrate the similarities and differences among the various stomatal models. Figure 4 shows simulations of g_w for the BB model as implemented in CLM4.5 using the global mean g_1 of 9 for all C_3 plants (Bonan et al., 2011). Also shown is the equivalent implementation of the MED model (Medlyn et al., 2011), with $g_{1M} = 4.45$ (kPa)$^{0.5}$ for broadleaf deciduous trees (Table II), and a water-use efficiency optimization (WUE) model (Bonan et al., 2014), with λ = 1.33 mmol water μmol^{-1} CO_2, which was evaluated by Bonan et al. (2014) for several broadleaf deciduous forests. An important point with regard to these simulations is that, although the equation for g_w in the MED model (Eq. 3) was derived for the condition of RuBP regeneration-limited CO_2 assimilation (A_j), when implemented in land surface models, A is commonly calculated as in Equation 6 (i.e. the minimum of A_c and A_j).

All three models show similar functional responses of stomatal conductance to light, CO_2, and temperature (Fig. 4, A, B, and D), although BB in this configuration has considerably lower stomatal conductance compared with the other two models. In all three models, stomatal conductance decreases with atmospheric CO_2 concentrations less than about 300 μL L^{-1}, as has been noted by others (Buckley et al., 2017). The model outputs in this case differ in their overall response to D_s (Fig. 4C). The BB simulation has a linear decline in

Table II. *Interchangeable water-use efficiency indexes*

Values for g_{1M} (see Eq. 3) are shown for different plant functional types, as used when implementing the Medlyn et al. (2011) stomatal model in CABLE (De Kauwe et al., 2015; Kala et al., 2015) and in the CLM4.5 simulations in Figures 9 and 10 below. These values are based on those given by Lin et al. (2015) but differ slightly in some cases. Equivalent approximate values are derived from g_{1M} for λ, g_1, and mean c_i/c_a using Equations 4, 5, and 9 (25°C, $H = 0.8$, $\Gamma^* = 40$ μmol mol^{-1}). In the model implementation, $g_0 = 0$, as was the case for Lin et al. (2015) when determining g_{1M} from gas-exchange data. Plant types with lower values for g_{1M}, g_1, λ, or c_i/c_a have comparatively higher water-use efficiency.

Plant Type	g_{1M}	g_1	λ	c_i/c_a
	$kPa^{0.5}$		*mmol water* μmol^{-1} CO_2	
C_3 crop	5.79	16.5	4.47	0.88
C_3 grass	5.25	15.1	3.68	0.87
Shrub	4.70	13.8	2.95	0.85
Deciduous broadleaf tree	4.45	13.1	2.64	0.85
Evergreen broadleaf tree	4.12	12.3	2.26	0.84
Evergreen needleleaf tree	2.35	7.88	0.74	0.75
Deciduous needleleaf tree	2.35	7.88	0.74	0.75
Arctic tundra	2.22	7.55	0.66	0.74
C_4 grass	1.62	6.05	0.35	0.67

stomatal conductance with increasing D_s, while MED and WUE have considerably higher stomatal conductance at low D_s, but this diminishes exponentially as D_s increases.

The differences in g_w simulated with the BB and MED models in Figure 4 result primarily from the prescribed values for g_1 and g_{1M} (9 and 4.45, respectively). When g_{1M} is reduced to 2.8 (kPa)$^{0.5}$ in MED and

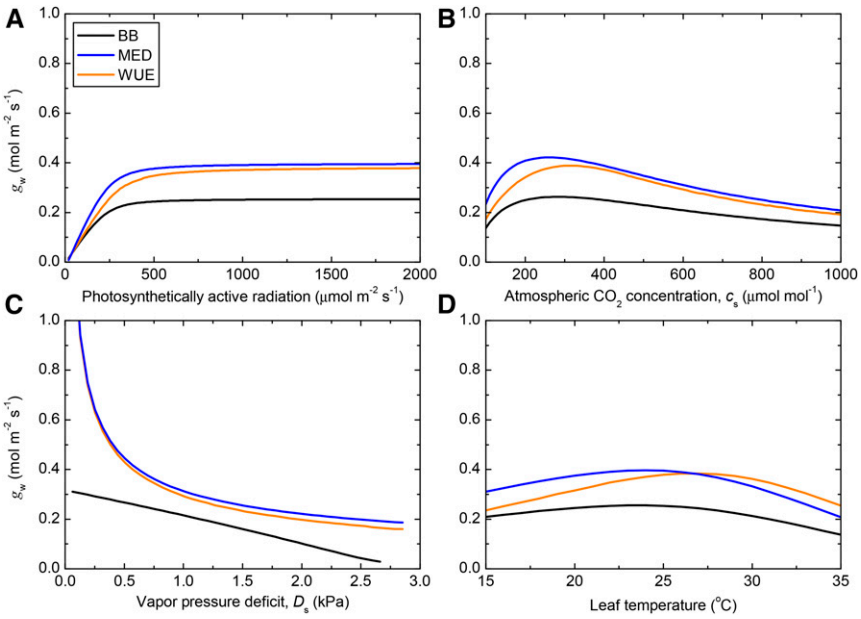

Figure 4. Simulations of leaf stomatal conductance, g_w, in response to photosynthetically active radiation (A), ambient CO_2 concentration at the leaf surface, c_s (B), vapor pressure deficit at the leaf surface at 101 kPa atmospheric pressure, D_s (C), and leaf temperature (D). Shown are results for the BB model (Eq. 1; Ball et al., 1987), with $g_0 = 0.01$ mol m^{-2} s^{-1} and $g_1 = 9$; the MED model (Eq. 3; Medlyn et al., 2011), with $g_0 = 0$ mol m^{-2} s^{-1} and $g_{1M} = 4.45$ (kPa)$^{0.5}$; and the WUE model (Bonan et al., 2014), with $\lambda = 1.33$ mmol water μmol^{-1} CO_2. All simulations used the Farquhar et al. (1980b) photosynthesis model as implemented in CLM4.5 (Bonan et al., 2011) with parameter values for the broadleaf deciduous tree plant functional type. The ratio of potential electron transport rate to maximum RuBP carboxylation rate, J_{max}/V_{cmax}, is 1.67 (at 25°C). Standard conditions for the simulations were as follows: $c_a = 380$ μmol mol^{-1}, photosynthetically active radiation = 2,000 μmol m^{-2} s^{-1} (or 0–2,000 μmol m^{-2} s^{-1} for g_w light responses), relative humidity = 0.8, air temperature = 25°C, and leaf temperature = 25°C. Environmental factors were varied individually. For the temperature simulation, vapor pressure was adjusted so that relative humidity remained constant (80%) or vapor pressure deficit remained constant (0.6 kPa) depending on the model. For these simulations, boundary layer conductance was 2 mol m^{-2} s^{-1}, so D_s is comparable to leaf-to-air vapor pressure difference.

g_1 is maintained at 9 in BB, the responses of g_w to light, CO_2, and temperature are nearly identical between the two models (Fig. 5, A, B, and D). Note that a g_{1M} of 2.8 $(kPa)^{0.5}$ is equivalent to a g_1 of 9, using Equation 5. Also, with these adjustments, the stomatal responses to D_s are nearly identical over the range 0.5 to 2 kPa (Fig. 5C). However, MED maintains a much larger stomatal conductance at low D_s compared with BB and higher stomatal conductance at larger D_s. For $D_s < 0.5$ kPa, MED has a much larger sensitivity to D_s than BB. For $D_s > 1.75$ kPa, MED is nearly invariant with D_s. In the WUE model, decreasing λ from 1.33 mmol water μmol^{-1} CO_2 in the default simulation (Fig. 4) to 0.714 mmol water μmol^{-1} CO_2 matches the WUE model output with the BB and MED models for light (Fig. 5A) and closely matches the WUE model with the MED model for D_s (Fig. 5C). The CO_2 response of the WUE model closely matches BB and MED model simulations at CO_2 concentrations greater than 300 $\mu L\ L^{-1}$ but diverges slightly from those models at lower CO_2. Buckley et al. (2017) also showed that the BB, MED, and an optimization model similar to the WUE model here can be formulated to produce similar results. The light, CO_2, and D_s simulations shown in Figure 5 are at a constant leaf temperature (25°C). When leaf temperature varies, the temperature response of g_w in the WUE model closely matches BB and MED (Fig. 5D), but only if $g_{1M} \propto \sqrt{\Gamma^* \lambda}$ (see Eq. 4; i.e. λ decreases with temperature according to the temperature dependence of Γ^*).

Although the BB and MED stomatal responses to CO_2 are similar, the WUE model estimates lower stomatal conductance with CO_2 concentrations less than 300 $\mu L\ L^{-1}$ (Fig. 5B). The results shown in Figures 4 and 5 are with a ratio of maximum potential electron transport rate to maximum RuBP carboxylation rate, J_{max}/V_{cmax}, of 1.67 (at 25°C). Decreasing the ratio J_{max}/V_{cmax} to 1.3 (at 25°C) and increasing λ slightly (from 0.714 to 0.909 mmol water μmol^{-1} CO_2 at 25°C) produces closer agreement among the three models for the response of g_w to CO_2 (Fig. 6B) while maintaining the same close agreement among the models for g_w response to light, D_s, and temperature (compare Fig. 5, A, C, and D, with Fig. 6, A, C, and D). The lower J_{max}/V_{cmax} ratio had little effect on the BB and MED model simulations, but in combination with the higher λ, it shifted the WUE model CO_2 curve to the left (compare Figs. 5B and 6B). This is because the lower J_{max}/V_{cmax} ratio places A in the RuBP regeneration-limited region of operation at a lower CO_2 concentration (Farquhar et al., 1980b), which aligns better with models like MED that represent g_w in terms of RuBP regeneration-limited photosynthesis. Simulations with $J_{max}/V_{cmax} = 2$ (at 25°C) further highlight this effect: in all three models, higher J_{max}/V_{cmax} shifts the CO_2 response curve for g_w to the right (Fig. 7).

The simulations in Figure 7 predict that stomatal sensitivity to an increase in atmospheric CO_2 concentration from 370 to 570 $\mu L\ L^{-1}$ declines with higher J_{max}/V_{cmax}. With $J_{max}/V_{cmax} = 1.67$, g_w declines by 16% to 20% (Figs. 4B and 5B; Table III). This is consistent with an approximately 20% reduction seen in free-air CO_2 enrichment studies as CO_2 increases from 370 to 570 $\mu L\ L^{-1}$ (Ainsworth and Rogers, 2007). With $J_{max}/V_{cmax} = 1.3$, the decline in stomatal conductance increases to 21% to 22% (Fig. 6B; Table III). With $J_{max}/V_{cmax} = 2$, the decline in stomatal conductance is only 6% to 12% over the same range of atmospheric CO_2 concentration (Fig. 7; Table III), but at higher CO_2 concentration, the decline is steeper. These results show that, for all models, the observed decline in g_w with elevated CO_2 is significantly influenced by the ratio J_{max}/V_{cmax}. They also highlight the potential influence of J_{max}/V_{cmax} and its plasticity in plants growing under different atmospheric CO_2 concentrations on the sensitivity of g_w to CO_2.

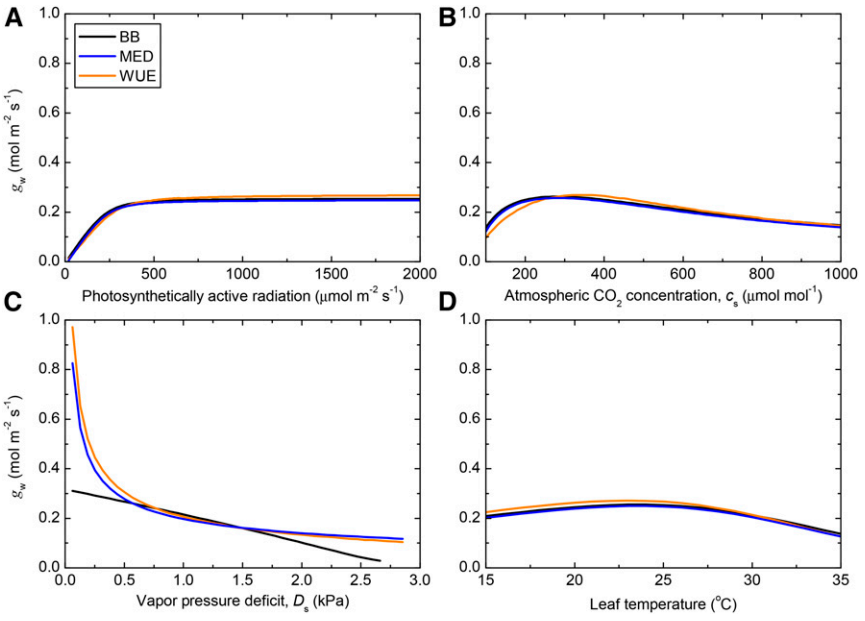

Figure 5. Using comparable g_1 and g_{1M} values results in similar outputs for the BB and MED models. Conditions were as in Figure 4, but with g_{1M} = 2.8 $(kPa)^{0.5}$ for MED and λ = 0.714 mmol water μmol^{-1} CO_2 for WUE.

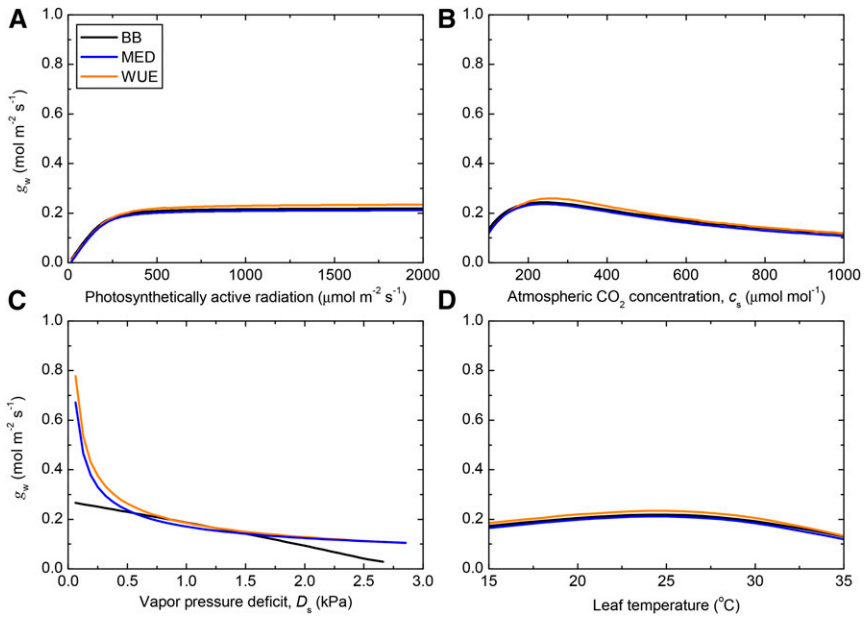

Figure 6. Effects of reducing J_{max}/V_{cmax} and increasing λ. Conditions were as in Figure 5, but J_{max}/V_{cmax} was reduced to 1.3 (at 25°C) and λ was increased slightly (from 0.714 to 0.909 mmol water μmol^{-1} CO_2 at 25°C).

Note that, in the simulations from the WUE model shown in Figures 4 to 7, photosynthesis is modeled as the colimited A_c and A_j rates. The effect of this colimitation is to smooth the transition between the A_c and A_j rates. Without colimitation, there is a sharp transition in stomatal conductance over a specific narrow range of atmospheric CO_2 concentration, seen prominently in high light. Buckley et al. (2017) found a similar discontinuity and suggested that it was an artifact in the optimization solution resulting from the characteristics of the Farquhar et al. (1980b) photosynthesis model that strictly represents photosynthesis at the scale of the chloroplast. The smooth CO_2 response curve for g_w obtained with the colimitation solution of water-use efficiency optimization is more physiologically representative of leaf and larger scales where the behavior of many millions of chloroplasts in slightly different microenvironments is integrated.

Canopy-Scale Simulations

Canopy-scale simulations with the BB, MED, and WUE models for a broadleaf deciduous forest further highlight the similarities among the models. Bonan et al. (2014) developed a multilayer canopy flux parameterization for use with CLM4.5 and evaluated the model at three broadleaf deciduous forest eddy covariance flux tower sites. We tested the three stomatal models (BB, MED, and WUE) in this framework in comparison with measured latent heat flux at Harvard Forest (US-Ha1 in Bonan et al., 2014). The BB model with g_1 = 9 underestimates midday latent heat flux compared with observations (Fig. 8A), MED [with the default g_{1M} = 4.45 (kPa)$^{0.5}$] simulates higher midday latent heat flux than the BB model and better matches the observations (Fig. 8B), and the WUE model (with the default λ = 1.33 mmol water μmol^{-1} CO_2) also simulates higher midday latent heat flux, fitting the data somewhere between the BB and MED models. This result is consistent with the leaf simulations shown in Figure 4, but all three model simulations when compared with the Harvard Forest data are within the observational uncertainty (blue shaded regions in Fig. 8).

Increasing g_1 in the BB model to 13 (to compare with g_{1M} = 4.45), decreasing g_{1M} in the MED model to 2.8 (kPa)$^{0.5}$ (to compare with g_1 = 9), and decreasing λ in the WUE model to 0.714 mmol water μmol^{-1} CO_2 (to compare with g_1 = 9) allows a more realistic comparison

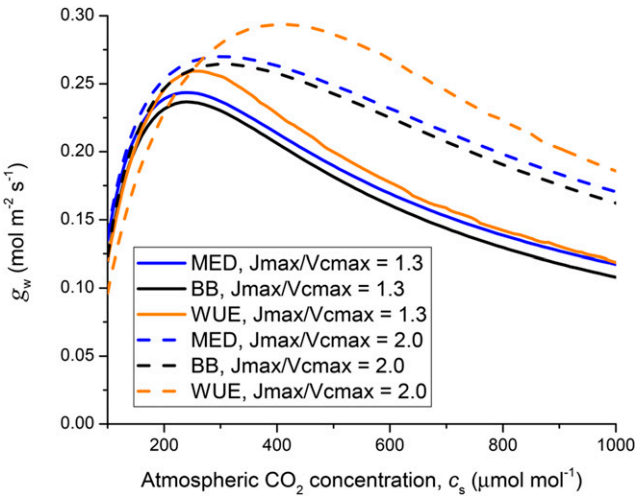

Figure 7. Influence of J_{max}/V_{cmax} on stomatal sensitivity to CO_2. Conditions were as in Figure 6, but with either J_{max}/V_{cmax} = 1.3 or 2 for the BB, MED, and WUE models.

Table III. *Stomatal sensitivity to CO_2*

Change in stomatal conductance (%) with an increase in atmospheric CO_2 concentration from 370 to 570 μL L^{-1} is shown for simulations using three different stomatal conductance models (BB, MED, and WUE), as configured for Figures 4 to 7.

Figure (J_{max}/V_{cmax})	BB (g_1)	MED (g_{1M})	WUE (λ)
4 (1.67)	−16 (9)	−19 (4.45)	−20 (1.330)
5 (1.67)	−16 (9)	−16 (2.80)	−17 (0.714)
6 (1.30)	−21 (9)	−22 (2.80)	−22 (0.909)
7 (2.00)	−11 (9)	−12 (2.80)	−6 (0.909)

between the models. With a g_1 value that aligns with the original g_{1M} value used in the MED model, the fit of the BB model simulation to the data improved and was almost identical to the well-fitting MED model simulation (compare Fig. 8, B and D). With g_{1M} and λ values adjusted to correspond with the g_1 value of 9 for the original poorly fitting simulation from the BB model, both the MED and WUE model simulations were degraded to similarly poor fits (compare Fig. 8, A with E and F). Therefore, it is evident that comparable parameterization of g_1, g_{1M}, and λ in the BB, MED, and WUE models, and in particular the BB and MED models, within the CLM4.5 land surface model can yield similarly good or poor fits to canopy-scale data from flux towers.

Global Simulations

Global simulations with the BB and MED models in CLM4.5 illustrate the potential influence that differences in the parameterization of g_1 and g_{1M}, respectively, can have on estimates of water cycle and carbon cycle fluxes. To explore this, we ran simulations using satellite phenology and atmospheric forcing data for 1991 to 2010 taken from the combined Climatic Research Unit and National Center for Environment Prediction (CRU-NCEP) data set (Le Quéré et al., 2016). Overall, there is good agreement between CLM4.5

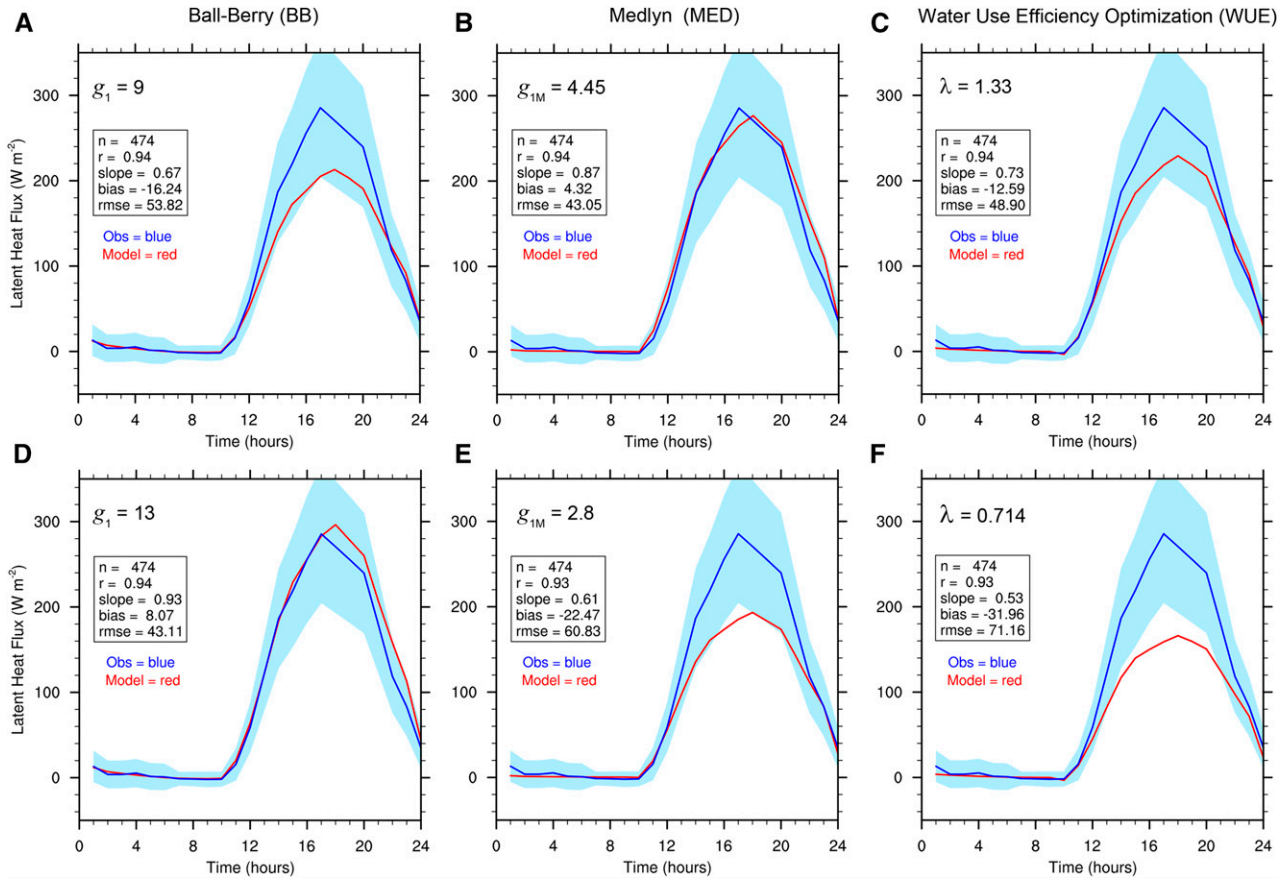

Figure 8. Comparison of canopy-scale simulations of latent heat flux, using the BB, MED, and WUE models, against flux tower data collected above the Harvard Forest study site, the Ameriflux network site US-Ha1 as described by Bonan et al. (2014). A, BB model with g_1 = 9. B, MED model with the default g_{1M} = 4.45 $(kPa)^{0.5}$. C, WUE model with the default λ = 1.33 mmol water μmol^{-1} CO_2. D, BB model with g_1 increased from 9 to 13. E, MED model with g_{1M} reduced from 4.45 to 2.8 $(kPa)^{0.5}$. F, WUE model with λ reduced from 1.33 to 0.714 mmol water μmol^{-1} CO_2. The blue shaded area is the 95% confidence interval for the flux tower data; the blue line is the mean for the flux tower data; and the red line is the simulated value from the BB, MED, or WUE model.

simulations using either the MED or BB stomatal conductance model (see light yellow areas in Figs. 9 and 10), but some regions show notable differences. CLM4.5 simulations using MED with the prescribed g_{1M} values for different plant types (Table II), relative to simulations using BB with a single prescribed global g_1 value of 9 for C3 plants and 4 for C4 plants, result in reduced gross primary productivity during summer in the western United States, north/central Asia, Europe, southern South America, and southern Australia (Fig. 9, A and C). In association, surface runoff during summer is lower in the eastern United States, northern Europe, southern Africa, and northern Australia (Fig. 9, B and D). Also, with this configuration, MED increases transpiration relative to BB in the tropics so that runoff decreases. Comparably large differences were seen with implementation of the MED model for g_w in CABLE (De Kauwe et al., 2015; Kala et al., 2015). Global simulations with JSBACH also showed differences, but neither the BB nor MED model reduces biases in model outputs (Knauer et al., 2015). In our simulations, these differences are reduced substantially when plant types in CLM4.5 simulations using the BB stomatal conductance model are assigned different g_1 values that correspond with the g_{1M} values for each plant type (Table II) rather than a single g_1 value of 9 for C3 plants (compare Fig. 9, A and C, with Fig. 10, A and C, respectively; and compare Fig. 9, B and D, with Fig. 10, B and D, respectively). The tropics are an exception, where transpiration increases further so that MED has higher surface runoff

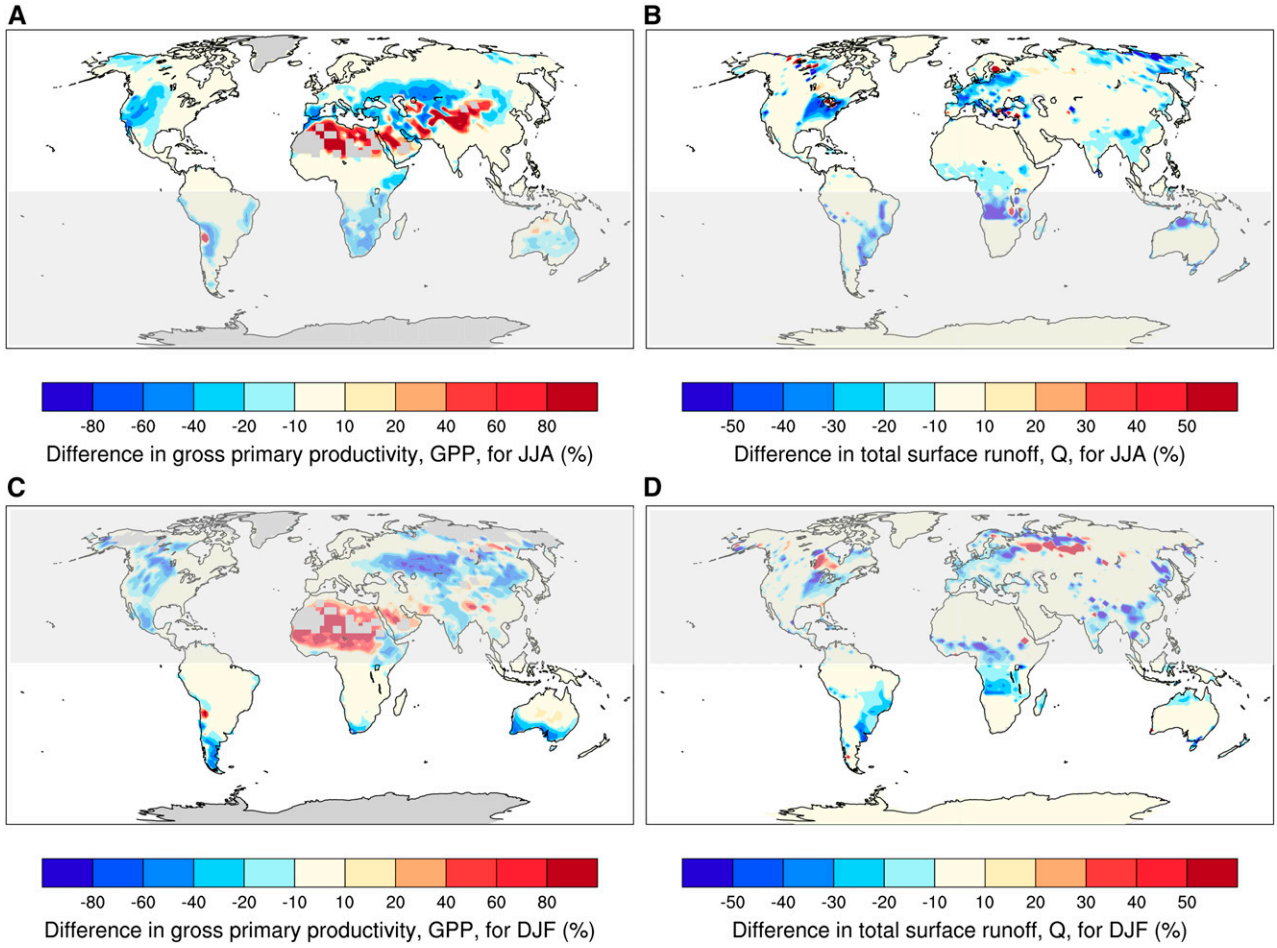

Figure 9. Effects of stomatal model parameterization on global simulations. Simulations were compared in the CLM4.5 global model incorporating the Medlyn et al. (2011) stomatal conductance model (MED; Eq. 3), configured with g_{1M} values listed in Table II, against CLM4.5 simulations using the BB stomatal conductance model (BB; Eq. 1), configured with a global mean g_1 value of 9 for C3 plants and 4 for C4 plants. The difference is calculated as 100(MED − BB)/BB. Data were generated by CLM4.5 using satellite phenology and Climatic Research Unit and National Center for Environment Prediction (CRU-NCEP) atmospheric forcing data for 1991 to 2010. A and B, Mean gross primary productivity (GPP) and total surface runoff (Q), respectively, for 3 months of the peak northern hemisphere summer growing season (June–August; JJA). C and D, As in A and B, but for the southern hemisphere summer growing season (December–February; DJF). To aid comparison, winter hemispheres are shaded translucent gray.

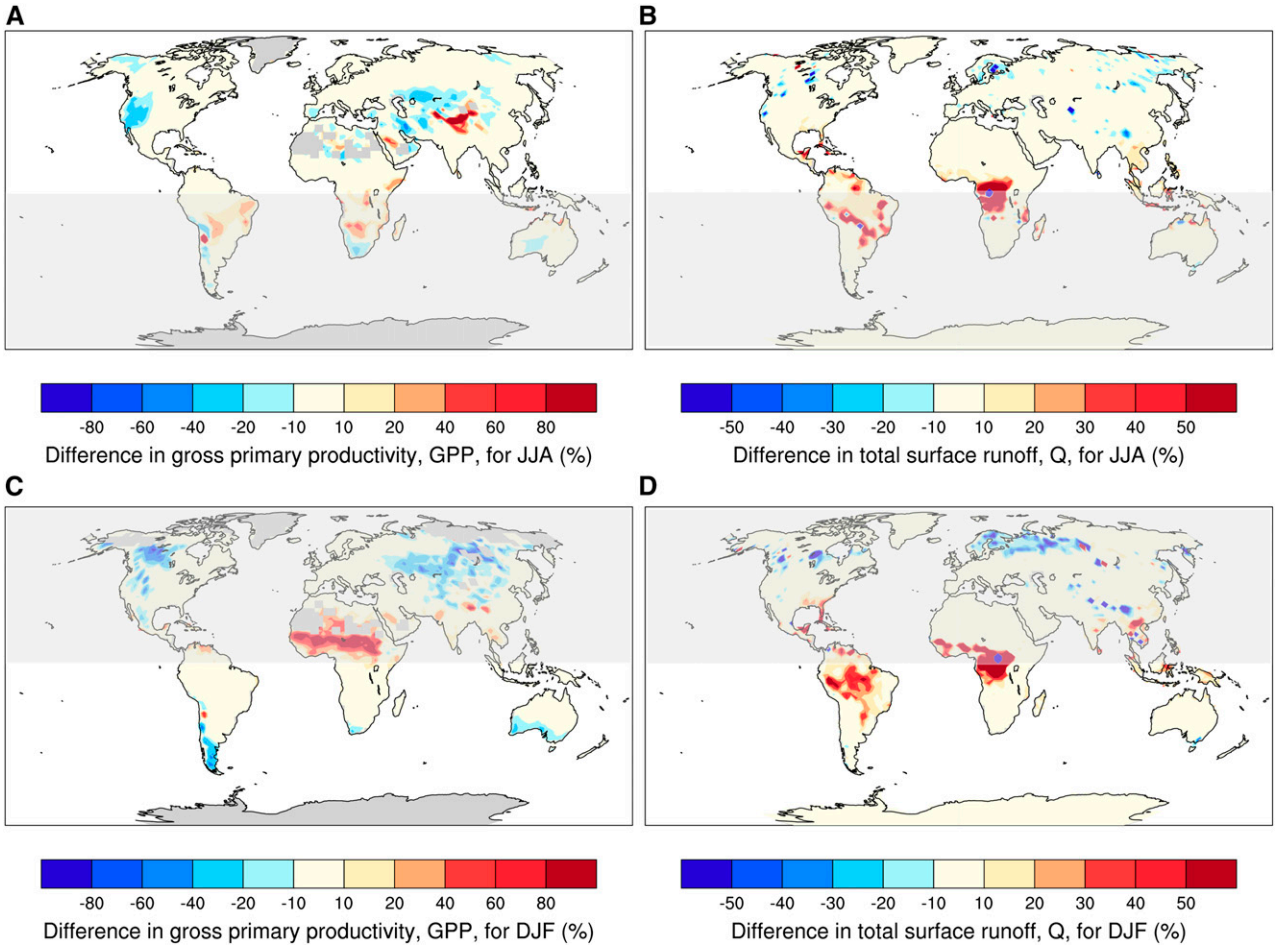

Figure 10. Similar parameterization of stomatal conductance models results in similar global simulations. The comparison of global simulations was as in Figure 9, except that instead of using a single mean g_1 value of 9 for simulations with the BB stomatal conductance model, different plant types were assigned individual values for g_1, derived from the g_{1M} values for those plant types using Equation 5 (Table II). This further improved the similarity between CLM4.5 simulations using either the BB or MED stomatal conductance model.

compared with the simulations using modified BB g_1 values (see orange-red shading in Fig. 10, B and D). As with our analyses for the leaf and canopy scales (Figs. 4–8), these global simulations show that vegetation models incorporating either the BB or MED model for stomatal conductance can produce similar outputs if the respective g_1 or g_{1M} parameters are assigned comparable values for similar plant types. In summary, the implementation of both empirical-based and optimization-based models of g_w in global land surface models results in equally good fits to observations; therefore, both methods are equally justified.

Accounting for Drought

The BB and MED style of stomatal conductance models is appropriate for well-watered soils in the absence of soil moisture stress. Less is known about how to represent stomatal closure in dry soils. Some models impose diffusive limitations in response to soil drying by reducing g_1, consistent with a shift to higher water-use efficiency or, at a more fundamental physiological level, reduced stomatal conductance under drought. Other models impose biochemical limitations and indirectly reduce stomatal conductance by reducing A as soil moisture stress increases (the models explicitly scale g_w with A; otherwise, water-use efficiency would decrease rather than increase with increased biochemical limitation on A). Neither approach can entirely replicate observations (Damour et al., 2010; Egea et al., 2011; De Kauwe et al., 2013), and possibly both diffusive and biochemical limitations must be considered (Zhou et al., 2013). There is also uncertainty about the form of the soil moisture stress function (Verhoef and Egea, 2014). As a result, there is considerable ongoing model development to implement in land surface models the process of plant water uptake and the effects of plant hydraulic stress on stomata (Bonan et al., 2014; Christoffersen et al., 2016; Xu et al., 2016).

OUTSTANDING QUESTIONS

- Uncertainty about the timing of emergence of basic stomatal sensitivities to CO_2 and the water stress hormone ABA is narrowing, but further physiological and genetic information is necessary to confirm the extent and activity of these mechanisms in the major vascular plant divisions.
- The evolutionary, environmental, and molecular processes that ultimately determine the critical stomatal conductance model parameters remain unknown.
- Accurately accounting for the effects of stomatal conductance at larger spatial scales, including "physiological forcing" of climate, remains a challenge.
- More accurate parameterization of current stomatal conductance models for use in global modeling will greatly improve simulations of global productivity, hydrology, and temperature and help address questions on the effects of global climate change.
- With current stomatal conductance models exhibiting similar capability in leaf, canopy, and global scale simulations, the immediate challenges are to (1) improve the parameterization of stomatal conductance models for application at multiple scales, including species-specific through to biome-specific parameters, (2) determine the plasticity and adaptability of stomatal conductance model parameters in response to sustained environmental change, and (3) improve representation of stomatal conductance response to soil water depletion and stress-induced changes in the hydraulic elements between soil and stomata.

CONCLUSION

The role of stomata in Earth system processes and the coevolution of this relationship have become increasingly apparent with new knowledge and better integration of geological, evolutionary, physiological, and global simulation data. Questions and challenges remain at each scale of investigation, but increasingly, there is a role for studies at one scale to inform another. Advances at the molecular level are addressing questions about the function and, in some cases, the mere presence of core elements of the stomatal conductance control mechanism and its behavior under multiple and often conflicting environmental signals (see Outstanding Questions). The integration of more realistic representation of stomatal conductance and its regulation of leaf gas exchange in global models is improving global simulations of carbon, water, and energy fluxes, and these simulations combined with observations in turn highlight some of the limitations with current leaf-scale models. Our analysis here of current leaf-scale models of stomatal conductance representing empirical-based or optimization-based approaches reveals close structural similarities that make them virtually interchangeable and indistinguishable in simulations of leaf, canopy, and global fluxes.

ACKNOWLEDGMENTS

We thank Tom Buckley for helpful comments.

Received February 24, 2017; accepted April 25, 2017; published April 26, 2017.

LITERATURE CITED

Ainsworth EA, Rogers A (2007) The response of photosynthesis and stomatal conductance to rising [CO_2]: mechanisms and environmental interactions. Plant Cell Environ **30:** 258–270

Andrews T, Doutriaux-Boucher M, Boucher O, Forster PM (2011) A regional and global analysis of carbon dioxide physiological forcing and its impact on climate. Clim Dyn **36:** 783–792

Arneth A, Harrison SP, Zaehle S, Tsigaridis K, Menon S, Bartlein PJ, Feichter J, Korhola A, Kulmala M, O'Donnell D, et al (2010) Terrestrial biogeochemical feedbacks in the climate system. Nat Geosci **3:** 525–532

Arneth A, Lloyd J, Šantrůčková H, Bird M, Grigoryyev S, Kalaschnikov YN, Gleixner G, Schulze E-D (2002) Response of central Siberian Scots pine to soil water deficit and long-term trends in atmospheric CO2 concentration. Global Biogeochemical Cycles **16:** 1005–1013

Bala G, Caldeira K, Wickett M, Phillips TJ, Lobell DB, Delire C, Mirin A (2007) Combined climate and carbon-cycle effects of large-scale deforestation. Proc Natl Acad Sci USA **104:** 6550–6555

Baldocchi D, Xu L (2005) Carbon exchange of deciduous broadleaved forests in temperate and Mediterranean regions. *In* H Griffiths, PG Jarvis, eds, The Carbon Balance of Forest Biomes. Taylor and Francis, New York, pp 187–214

Ball JT, Woodrow IE, Berry JA (1987) A model predicting stomatal conductance and its contribution to the control of photosynthesis under different environmental conditions. Prog Photosynth Res **4:** 221–224

Beaulieu JM, Leitch IJ, Patel S, Pendharkar A, Knight CA (2008) Genome size is a strong predictor of cell size and stomatal density in angiosperms. New Phytol **179:** 975–986

Beerling DJ (2007) The Emerald Planet: How Plants Changed Earth's History. Oxford University Press, Oxford, UK

Beerling DJ (2015) Gas valves, forests and global change: a commentary on Jarvis (1976) 'The interpretation of the variations in leaf water potential and stomatal conductance found in canopies in the field'. Philos Trans R Soc Lond B Biol Sci **370:** 20140311

Beerling DJ, Royer DL (2002) Reading a CO_2 signal from fossil stomata. New Phytol **153:** 387–397

Beerling DJ, Taylor LL, Bradshaw CDC, Lunt DJ, Valdes PJ, Banwart SA, Pagani M, Leake JR (2012) Ecosystem CO_2 starvation and terrestrial silicate weathering: mechanisms and global-scale quantification during the late Miocene. J Ecol **100:** 31–41

Beerling DJ, Woodward FI (1997) Changes in land plant function over the Phanerozoic: reconstructions based on the fossil record. Bot J Linn Soc **124:** 137–153

Berg A, Findell K, Lintner B, Giannini A, Seneviratne SI, van den Hurk B, Lorenz R, Pitman A, Hagemann S, Meier A, et al (2016) Land-atmosphere feedbacks amplify aridity increase over land under global warming. Nat Clim Chang **6:** 869–874

Berner RA (1997) The rise of plants and their effect on weathering and atmospheric CO_2. Science **276:** 544–546

Berner RA (2005) The rise of trees and how they changed paleozoic atmospheric CO_2, climate, and geology. *In* JR Ehleringer, T Cerling, MD Dearing, eds, A History of Atmospheric CO_2 and Its Effects on Plants, Animals, and Ecosystems. Springer-Verlag, New York, pp 1–7

Berry JA, Beerling DJ, Franks PJ (2010) Stomata: key players in the earth system, past and present. Curr Opin Plant Biol **13:** 233–240

Betts RA, Cox PM, Lee SE, Woodward FI (1997) Contrasting physiological and structural vegetation feedbacks in climate change simulations. Nature **387:** 796–799

Bonan GB (1995) Land-atmosphere CO_2 exchange simulated by a land surface process model coupled to an atmospheric general circulation model. J Geophys Res **100D:** 2817–2831

Bonan GB (2008) Forests and climate change: forcings, feedbacks, and the climate benefits of forests. Science **320:** 1444–1449

Bonan GB (2016) Ecological Climatology. Cambridge University Press, New York

Bonan GB, Lawrence PJ, Oleson KW, Levis S, Jung M, Reichstein M, Lawrence DM, Swenson SC (2011) Improving canopy processes in the Community Land Model version 4 (CLM4) using global flux fields empirically inferred from FLUXNET data. J Geophys Res **116:** G02014

Bonan GB, Pollard D, Thompson SL (1992) Effects of boreal forest vegetation on global climate. Nature **359:** 716–718

Bonan GB, Williams M, Fisher RA, Oleson KW (2014) Modeling stomatal conductance in the earth system: linking leaf water-use efficiency and water transport along the soil-plant-atmosphere continuum. Geosci Model Dev **7:** 2193–2222

Brodribb TJ, McAdam SAM (2011) Passive origins of stomatal control in vascular plants. Science **331:** 582–585

Brodribb TJ, McAdam SAM (2013) Unique responsiveness of angiosperm stomata to elevated CO_2 explained by calcium signalling. PLoS ONE **8:** e82057

Brodribb TJ, McAdam SAM, Jordan GJ, Feild TS (2009) Evolution of stomatal responsiveness to CO_2 and optimization of water-use efficiency among land plants. New Phytol **183:** 839–847

Buckley TN (2008) The role of stomatal acclimation in modelling tree adaptation to high CO_2. J Exp Bot **59:** 1951–1961

Buckley TN, Miller JM, Farquhar GD (2002) The mathematics of linked optimisation for water and nitrogen use in a canopy. Silva Fenn **36:** 639–669

Buckley TN, Mott KA, Farquhar GD (2003) A hydromechanical and biochemical model of stomatal conductance. Plant Cell Environ **26:** 1767–1785

Buckley TN, Sack L, Farquhar GD (2017) Optimal plant water economy. Plant Cell Environ **140:** 881–896

Buckley TN, Schymanski SJ (2014) Stomatal optimisation in relation to atmospheric CO_2. New Phytol **201:** 372–377

Byrne MP, O'Gorman PA (2016) Understanding decreases in land relative humidity with global warming: conceptual model and GCM simulations. J Clim **29:** 9045–9061

Cai S, Chen G, Wang Y, Huang Y, Marchant B, Wang Y, Yang Q, Dai F, Hills A, Franks PJ, et al (2017) Evolutionary conservation of ABA signaling for stomatal closure in ferns. Plant Physiol pp.01848.2016 (in press)

Cao L, Bala G, Caldeira K, Nemani R, Ban-Weiss G (2010) Importance of carbon dioxide physiological forcing to future climate change. Proc Natl Acad Sci USA **107:** 9513–9518

Chater C, Kamisugi Y, Movahedi M, Fleming A, Cuming AC, Gray JE, Beerling DJ (2011) Regulatory mechanism controlling stomatal behavior conserved across 400 million years of land plant evolution. Curr Biol **21:** 1025–1029

Chater CC, Caine RS, Tomek M, Wallace S, Kamisugi Y, Cuming AC, Lang D, MacAlister CA, Casson S, Bergmann DC, et al (2016) Origin and function of stomata in the moss *Physcomitrella patens*. Nat Plants **2:** 16179

Chen ZH, Chen G, Dai F, Wang Y, Hills A, Ruan YL, Zhang G, Franks PJ, Nevo E, Blatt MR (2017) Molecular evolution of grass stomata. Trends Plant Sci **22:** 124–139

Chen ZH, Hills A, Bätz U, Amtmann A, Lew VL, Blatt MR (2012) Systems dynamic modeling of the stomatal guard cell predicts emergent behaviors in transport, signaling, and volume control. Plant Physiol **159:** 1235–1251

Christoffersen BO, Gloor M, Fauset S, Fyllas NM, Galbraith DR, Baker TR, Kruijt B, Rowland L, Fisher RA, Binks OJ, et al (2016) Linking hydraulic traits to tropical forest function in a size-structured and trait-driven model (TFS v.1-Hydro). Geosci Model Dev **9:** 4227–4255

Collatz GJ, Ball JT, Grivet C, Berry JA (1991) Physiological and environmental-regulation of stomatal conductance, photosynthesis and transpiration: a model that includes a laminar boundary-layer. Agric For Meteorol **54:** 107–136

Cowan IR (2002) Fit, fitter, fittest: where does optimisation fit in? Silva Fenn **36:** 745–754

Cowan IR, Farquhar GD (1977) Stomatal function in relation to leaf metabolism and environment. *In* DH Jennings, ed, Integration of Activity in the Higher Plant: Symposia of the Society for Experimental Biology. Cambridge University Press, Cambridge, UK, pp 471–505

Cox PM, Huntingford C, Harding RJ (1998) A canopy conductance and photosynthesis model for use in a GCM land surface scheme. J Hydrol (Amst) **212-213:** 79–94

Crowell JC (1978) Gondwanan glaciation, cyclotherms, continental positioning, and climate change. Am J Sci **278:** 1345–1372

Damour G, Simonneau T, Cochard H, Urban L (2010) An overview of models of stomatal conductance at the leaf level. Plant Cell Environ **33:** 1419–1438

de Boer HJ, Price CA, Wagner-Cremer F, Dekker SC, Franks PJ, Veneklaas EJ (2016) Optimal allocation of leaf epidermal area for gas exchange. New Phytol **210:** 1219–1228

De Kauwe MG, Kala J, Lin YS, Pitman AJ, Medlyn BE, Duursma RA, Abramowitz G, Wang YP, Miralles DG (2015) A test of an optimal stomatal conductance scheme within the CABLE land surface model. Geosci Model Dev **8:** 431–452

De Kauwe MG, Medlyn BE, Zaehle S, Walker AP, Dietze MC, Hickler T, Jain AK, Luo Y, Parton WJ, Prentice IC, et al (2013) Forest water use and water use efficiency at elevated CO_2 : a model-data intercomparison at two contrasting temperate forest FACE sites. Glob Change Biol **19:** 1759–1779

Dickinson RE, Henderson-Sellers A, Kennedy PJ, Wilson MF (1986) Biosphere-Atmosphere Transfer Scheme (BATS) for the NCAR Community Climate Model. Technical Note NCAR/TN-275+STR. National Center for Atmospheric Research, Boulder, CO

Diefendorf AF, Mueller KE, Wing SL, Koch PL, Freeman KH (2010) Global patterns in leaf ^{13}C discrimination and implications for studies of past and future climate. Proc Natl Acad Sci USA **107:** 5738–5743

Doheny-Adams T, Hunt L, Franks PJ, Beerling DJ, Gray JE (2012) Genetic manipulation of stomatal density influences stomatal size, plant growth and tolerance to restricted water supply across a growth carbon dioxide gradient. Philos Trans R Soc Lond B Biol Sci **367:** 547–555

Dow GJ, Berry JA, Bergmann DC (2014) The physiological importance of developmental mechanisms that enforce proper stomatal spacing in *Arabidopsis thaliana*. New Phytol **201:** 1205–1217

Edwards D (1998) Climate signals in Paleozoic land plants. Philos Trans R Soc Lond B Biol Sci **353:** 141–156

Edwards D, Kerp H, Hass H (1998) Stomata in early land plants: an anatomical and ecophysiological approach. J Exp Bot **49:** 255–278

Egea G, Verhoef A, Vidale PL (2011) Towards an improved and more flexible representation of water stress in coupled photosynthesis-stomatal conductance models. Agric For Meteorol **151:** 1370–1384

Farquhar GD, Ehleringer JR, Hubick KT (1989) Carbon isotope discrimination and photosynthesis. Annu Rev Plant Physiol Plant Mol Biol **40:** 503–537

Farquhar GD, Schulze ED, Kuppers M (1980a) Responses to humidity by stomata of *Nicotiana glauca* L. and *Corylus avellana* L. are consistent with the optimization of carbon dioxide uptake with respect to water loss. Aust J Plant Physiol **7:** 315–327

Farquhar GD, Sharkey TD (1982) Stomatal conductance and photosynthesis. Annu Rev Plant Physiol **33:** 17–45

Farquhar GD, von Caemmerer S, Berry JA (1980b) A biochemical model of photosynthetic CO_2 assimilation in leaves of C 3 species. Planta **149:** 78–90

Feddema JJ, Oleson KW, Bonan GB, Mearns LO, Buja LE, Meehl GA, Washington WM (2005) The importance of land-cover change in simulating future climates. Science **310:** 1674–1678

Feng X (1999) Trends in intrinsic water-use efficiency of natural trees for the past 100–200 years: a response to atmospheric CO_2 concentration. Geochim Cosmochim Acta **63:** 1891–1903

Franks PJ (2013) Passive and active stomatal control: either or both? New Phytol **198:** 325–327

Franks PJ, Adams MA, Amthor JS, Barbour MM, Berry JA, Ellsworth DS, Farquhar GD, Ghannoum O, Lloyd J, McDowell N, et al (2013) Sensitivity of plants to changing atmospheric CO_2 concentration: from the geological past to the next century. New Phytol **197:** 1077–1094

Franks PJ, Beerling DJ (2009a) CO_2-forced evolution of plant gas exchange capacity and water-use efficiency over the Phanerozoic. Geobiology **7:** 227–236

Franks PJ, Beerling DJ (2009b) Maximum leaf conductance driven by CO_2 effects on stomatal size and density over geologic time. Proc Natl Acad Sci USA **106:** 10343–10347

Franks PJ, Britton-Harper ZJ (2016) No evidence of general CO_2 insensitivity in ferns: one stomatal control mechanism for all land plants? New Phytol **211:** 819–827

Franks PJ, Doheny-Adams T, Britton-Harper ZJ, Gray JE (2015) Increasing water-use efficiency directly through genetic manipulation of stomatal density. New Phytol **207:** 188–195

Franks PJ, Drake PL, Beerling DJ (2009) Plasticity in maximum stomatal conductance constrained by negative correlation between stomatal size and density: an analysis using *Eucalyptus globulus*. Plant Cell Environ **32:** 1737–1748

Franks PJ, Farquhar GD (1999) A relationship between humidity response, growth form and photosynthetic operating point in C3 plants. Plant Cell Environ **22:** 1337–1349

Franks PJ, Farquhar GD (2007) The mechanical diversity of stomata and its significance in gas-exchange control. Plant Physiol **143:** 78–87

Franks PJ, Freckleton RP, Beaulieu JM, Leitch IJ, Beerling DJ (2012a) Megacycles of atmospheric carbon dioxide concentration correlate with fossil plant genome size. Philos Trans R Soc Lond B Biol Sci **367:** 556–564

Franks PJ, Leitch IJ, Ruszala EM, Hetherington AM, Beerling DJ (2012b) Physiological framework for adaptation of stomata to CO_2 from glacial to future concentrations. Philos Trans R Soc Lond B Biol Sci **367:** 537–546

Franks PJ, Royer DL, Beerling DJ, van de Water PK, Cantrill DJ, Barbour MM, Berry JA (2014) New constraints on atmospheric CO_2 concentration for the Phanerozoic. Geophys Res Lett **41:** 4685–4694

Geisler M, Nadeau J, Sack FD (2000) Oriented asymmetric divisions that generate the stomatal spacing pattern in *Arabidopsis* are disrupted by the *too many mouths* mutation. Plant Cell **12:** 2075–2086

Grein M, Konrad W, Wilde V, Utescher T, Roth-Nebelsick A (2011) Reconstruction of atmospheric CO_2 during the early middle Eocene by application of a gas exchange model to fossil plants from the Messel Formation, Germany. Palaeogeogr Palaeoclimatol Palaeoecol **309:** 383–391

Haworth M, Killi D, Materassi A, Raschi A (2015) Coordination of stomatal physiological behavior and morphology with carbon dioxide determines stomatal control. Am J Bot **102:** 677–688

Hetherington AM, Woodward FI (2003) The role of stomata in sensing and driving environmental change. Nature **424:** 901–908

Hills A, Chen ZH, Amtmann A, Blatt MR, Lew VL (2012) OnGuard, a computational platform for quantitative kinetic modeling of guard cell physiology. Plant Physiol **159:** 1026–1042

Jarvis PG (1976) The interpretation of the variations in leaf water potential and stomatal conductance found in canopies in the field. Philos Trans R Soc Lond B Biol Sci **273:** 593–610

Kala J, De Kauwe MG, Pitman AJ, Lorenz R, Medlyn BE, Wang YP, Lin YS, Abramowitz G (2015) Implementation of an optimal stomatal conductance scheme in the Australian Community Climate Earth Systems Simulator (ACCESS1.3b). Geosci Model Dev **8:** 3877–3889

Kaminski KP, Kørup K, Kristensen K, Nielsen KL, Liu F, Topbjerg HB, Kirk HG, Andersen MN (2015) Contrasting water-use efficiency (WUE) responses of a potato mapping population and capability of modified Ball-Berry model to predict stomatal conductance and WUE measured at different environmental conditions. J Agron Crop Sci **201:** 81–94

Katul G, Manzoni S, Palmroth S, Oren R (2010) A stomatal optimization theory to describe the effects of atmospheric CO_2 on leaf photosynthesis and transpiration. Ann Bot (Lond) **105:** 431–442

Katul GG, Palmroth S, Oren R (2009) Leaf stomatal responses to vapour pressure deficit under current and CO_2-enriched atmosphere explained by the economics of gas exchange. Plant Cell Environ **32:** 968–979

Kiehl JT, Shields CA (2013) Sensitivity of the Palaeocene-Eocene thermal maximum climate to cloud properties. Philos Trans A Math Phys Eng Sci **371:** 20130093

Kleidon A, Fraedrich K, Heimann M (2000) A green planet versus a desert world: estimating the maximum effect of vegetation on the land surface. Clim Change **44:** 471–493

Knauer J, Werner C, Zaehle S (2015) Evaluating stomatal models and their atmospheric drought response in a land surface scheme: a multibiome analysis. J Geophys Res Biogeosci **120:** 1894–1911

Knight CA, Beaulieu JM (2008) Genome size scaling through phenotype space. Ann Bot (Lond) **101:** 759–766

Konrad W, Roth-Nebelsick A, Grein M (2008) Modelling of stomatal density response to atmospheric CO_2. J Theor Biol **253:** 638–658

Le Quéré C, Andrew RM, Canadell JG, Sitch S, Korsbakken JI, Peters GP, Manning AC, Boden TA, Tans PP, Houghton RA, et al (2016) Global Carbon Budget 2016. Earth Syst Sci Data **8:** 605–649

Leuning R (1990) Modelling stomatal behaviour and photosynthesis of *Eucalyptus grandis*. Aust J Plant Physiol **17:** 159–175

Leuning R (1995) A critical appraisal of a combined stomatal-photosynthesis model. Plant Cell Environ **18:** 339–355

Lin YS, Medlyn BE, Duursma RA, Prentice IC, Wang H, Baig S, Eamus D, Resco de Dios V, Mitchell P, Ellsworth DS, et al (2015) Optimal stomatal behaviour around the world. Nat Clim Chang **5:** 459–464

Lind C, Dreyer I, López-Sanjurjo EJ, von Meyer K, Ishizaki K, Kohchi T, Lang D, Zhao Y, Kreuzer I, Al-Rasheid KA, et al (2015) Stomatal guard cells co-opted an ancient ABA-dependent desiccation survival system to regulate stomatal closure. Curr Biol **25:** 928–935

Lloyd J (1991) Modelling stomatal response to environment in *Macadamia integrifolia*. Aust J Plant Physiol **18:** 649–660

Lloyd J, Farquhar GD (1994) ^{13}C discrimination during CO_2 assimilation by the terrestrial biosphere. Oecologia **99:** 201–215

Lowry DP, Poulsen CJ, Horton DE, Torsvik TH, Pollard D (2014) Thresholds for Paleozoic ice sheet initiation. Geology **42:** 627–630

McAdam SAM, Brodribb TJ (2012) Fern and lycophyte guard cells do not respond to endogenous abscisic acid. Plant Cell **24:** 1510–1521

McAdam SAM, Brodribb TJ (2015) The evolution of mechanisms driving the stomatal response to vapor pressure deficit. Plant Physiol **167:** 833–843

McAdam SAM, Brodribb TJ, Banks JA, Hedrich R, Atallah NM, Cai C, Geringer MA, Lind C, Nichols DS, Stachowski K, et al (2016) Abscisic acid controlled sex before transpiration in vascular plants. Proc Natl Acad Sci USA **113:** 12862–12867

McElwain JC, Beerling DJ, Woodward FI (1999) Fossil plants and global warming at the Triassic-Jurassic boundary. Science **285:** 1386–1390

McInerney FA, Wing SL (2011) The Paleocene-Eocene thermal maximum: a perturbation of carbon cycle, climate, and biosphere with implications for the future. Annu Rev Earth Planet Sci **39:** 489–516

Medlyn BE, Duursma RA, Eamus D, Ellsworth DS, Prentice IC, Barton CVM, Crous KY, de Angelis P, Freeman M, Wingate L (2011) Reconciling the optimal and empirical approaches to modelling stomatal conductance. Glob Change Biol **17:** 2134–2144

Meissner KJ, Bralower TJ, Alexander K, Jones TD, Sijp W, Ward M (2014) The Paleocene-Eocene thermal maximum: how much carbon is enough? Paleoceanography **29:** 946–963

Montañez IP, McElwain JC, Poulsen CJ, White JD, DiMichele WA, Wilson JP, Griggs G, Hren MT (2016) Climate, pCO_2 and terrestrial carbon cycle linkages during late Palaeozoic glacial-interglacial cycles. Nat Geosci **9:** 824–828

Montañez IP, Poulsen CJ (2013) The late Paleozoic ice age: an evolving paradigm. Annu Rev Earth Planet Sci **41:** 629–656

Oleson KW, Lawrence DM, Bonan GB, Drewniak B, Huang MK, Levis S, Li F, Riley WJ, Subin ZM, Swenson SC, et al (2013) Technical Description of Version 4.5 of the Community Land Model (CLM). National Center for Atmospheric Research, Boulder, CO

Pagani M, Caldeira K, Berner R, Beerling DJ (2009) The role of terrestrial plants in limiting atmospheric CO_2 decline over the past 24 million years. Nature **460:** 85–88

Raven JA (2002) Selection pressures on stomatal evolution. New Phytol **153:** 371–386

Reid CD, Maherali H, Johnson HB, Smith SD, Wullschleger SD, Jackson RB (2003) On the relationship between stomatal characters and atmospheric CO_2. Geophys Res Lett **30:** 1983

Royer DL (2014) Atmospheric CO2 and O2 during the Phanerozoic: tools, patterns, and impacts. *In* Treatise on Geochemistry, Ed 2. Holland H, Turekian K, eds, Elsevier, Amsterdam, The Netherlands pp 251–267

Royer DL, Berner RA, Montañez IP, Tabor NJ, Beerling DJ (2004) CO_2 as a primary driver of Phanerozoic climate. GSA Today **14:** 4–10

Russo SE, Cannon WL, Elowsky C, Tan S, Davies SJ (2010) Variation in leaf stomatal traits of 28 tree species in relation to gas exchange along an edaphic gradient in a Bornean rain forest. Am J Bot **97:** 1109–1120

Ruszala EM, Beerling DJ, Franks PJ, Chater C, Casson SA, Gray JE, Hetherington AM (2011) Land plants acquired active stomatal control early in their evolutionary history. Curr Biol **21:** 1030–1035

Scheffler K, Hoernes S, Schwark L (2003) Global changes during Carboniferous-Permian glaciation of Gondwana: linking polar and equatorial climate evolution by geochemical proxies. Geology **31:** 605–608

Schulze ED, Kelliher FM, Korner C, Lloyd J, Leuning R (1994) Relationships among maximum stomatal conductance, ecosystem surface conductance, carbon assimilation rate, and plant nitrogen nutrition. Annu Rev Ecol Syst **25:** 629–660

Sellers PJ, Bounoua L, Collatz GJ, Randall DA, Dazlich DA, Los SO, Berry JA, Fung I, Tucker CJ, Field CB, et al (1996a) Comparison of radiative and physiological effects of doubled atmospheric CO_2 on climate. Science **271:** 1402–1406

Sellers PJ, Mintz Y, Sud YC, Dalcher A (1986) A simple biosphere model (SiB) for use within general circulation models. J Atmos Sci **43:** 505–531

Sellers PJ, Randall DA, Collatz GJ, Berry CM, Field CB, Dalzich DA, Zhang C, Collelo GD, Bounoua L (1996b) A revised land surface parameterization (SiB2) for atmospheric GCMs. Part I. Model formulation. J Clim **9:** 676–705

Snyder PK, Delire C, Foley JA (2004) Evaluating the influence of different vegetation biomes on the global climate. Clim Dyn **23:** 279–302

Tricker PJ, Trewin H, Kull O, Clarkson GJJ, Eensalu E, Tallis MJ, Colella A, Doncaster CP, Sabatti M, Taylor G (2005) Stomatal conductance and not stomatal density determines the long-term reduction in leaf transpiration of poplar in elevated CO_2. Oecologia **143:** 652–660

Upchurch GR, Kiehl J, Shields C, Scherer J, Scotese C (2015) Latitudinal temperature gradients and high-latitude temperatures during the latest Cretaceous: congruence of geologic data and climate models. Geology **43:** 683–686

Verhoef A, Egea G (2014) Modeling plant transpiration under limited soil water: comparison of different plant and soil hydraulic parameterizations and preliminary implications for their use in land surface models. Agric For Meteorol **191:** 22–32

Vico G, Manzoni S, Palmroth S, Weih M, Katul G (2013) A perspective on optimal leaf stomatal conductance under CO_2 and light co-limitations. Agric For Meteorol **182-183:** 191–199

Wang H, Dittmer TA, Richards EJ (2013) Arabidopsis CROWDED NUCLEI (CRWN) proteins are required for nuclear size control and heterochromatin organization. BMC Plant Biol **13:** 200

Wang Y, Hills A, Blatt MR (2014) Systems analysis of guard cell membrane transport for enhanced stomatal dynamics and water use efficiency. Plant Physiol **164:** 1593–1599

Wang YP, Kowalczyk E, Leuning R, Abramowitz G, Raupach MR, Pak B, van Gorsel E, Luhar A (2011) Diagnosing errors in a land surface model (CABLE) in the time and frequency domains. J Geophys Res Biogeosci **116:** G01034

Woodward FI (1987) Stomatal numbers are sensitive to increases in CO_2 from preindustrial levels. Nature **327:** 617–618

Xu X, Medvigy D, Powers JS, Becknell JM, Guan K (2016) Diversity in plant hydraulic traits explains seasonal and inter-annual variations of vegetation dynamics in seasonally dry tropical forests. New Phytol **212:** 80–95

Zhou S, Duursma RA, Medlyn BE, Kelly JWG, Prentice IC (2013) How should we model plant responses to drought? An analysis of stomatal and non-stomatal responses to water stress. Agric For Meteorol **182–183:** 204–214